Interactions of plutons and detachments, comparison of Aegean and Tyrrhenian granitoids

Laurent Jolivet [1], Laurent Arbaret [2,3,4], Laetitia Le Pourhiet [1], Florent Cheval-Garabedian [2,3,4], Vincent Roche [1], Aurélien Rabillard [2,3,4], Loïc Labrousse [1]

[1] Sorbonne Université, CNRS-INSU, Institut des Sciences de la Terre Paris, ISTeP UMR 7193, F-75005 Paris, France

[2] Université d'Orléans, ISTO, UMR 7327, 45071, Orléans, France

[3] CNRS/INSU, ISTO, UMR 7327, 45071 Orléans, France

[4] BRGM, ISTO, UMR 7327, BP 36009, 45060 Orléans, France

Abstract: Back-arc extension superimposed on mountain belts leads to distributed normal faults and shear zones interacting with magma emplacement within the crust. The composition of granitic magmas emplaced at this stage often involves a large component of crustal melting. The Miocene Aegean granitoids were emplaced in metamorphic core complexes (MCC) below crustal-scale low-angle normal faults and ductile shear zones. Intrusion processes interact with extension and shear along detachments, from the hot magmatic flow within the pluton root zone to the colder ductile and brittle deformation below and along the detachment. A comparison of the Aegean plutons with the Elba Island MCC in the back-arc region of the Apennines subduction shows that these processes are characteristic of pluton-detachment interactions in general. We discuss a conceptual emplacement model, tested by numerical models. Mafic injections within the partially molten lower crust above the hot asthenosphere trigger the ascent within the core of the MCC of felsic magmas, controlled by the strain localization on persistent crustal scale shear zones at the top that guide the ascent until the brittle ductile transition. Once the system definitely enters the brittle regime, the detachment and the upper crust are intruded, while new detachments migrate upward and in the direction of shearing.

1. Introduction

In the deep parts of orogens, the flow of melts is coupled with ductile deformation and controlled by buoyancy and tectonic forces (Brown, 1994; Brown and Solar, 1998; Brown, 2007). Migmatites, which are weak crustal material as long as they are kept at high temperature, are the source of magma batches that concentrate within plutons of various sizes. On the other hand, interactions between magmatism and lithospheric deformation, and more specifically interactions of plutons with crustal-scale tectonics, depend first of all upon the rate of magma production and, to a second order, to strain rates. The rate of magma transfer to the crust is indeed so large compared to tectonic strain rates that the construction of plutons is thought in a first approach to be little influenced by the tectonic setting, especially when small plutons are concerned (de Saint Blanquat et al., 2011).

The Miocene Aegean plutons (figure 1, figure 2), emplaced in an extensional context within metamorphic core complexes (MCCs), may however depart from this general behaviour. Despite a moderate volume, they have indeed recorded the complete evolution from syn-tectonic magmatic flow to localized mylonitic deformation along the main detachment (Faure and Bonneau, 1988; Urai et al., 1990; Faure et al., 1991; Lee and Lister, 1992; Gautier et al., 1993; Laurent et al., 2015; Rabillard et al., 2015; Bessière et al., 2017; Rabillard et al., 2018). All of them moreover show a systematic magmatic and tectonic evolution of the host MCCs with several magmatic pulses and a series of detachments forming sequentially during exhumation (Rabillard et al., 2018). Several of them also show an association of mixed or mingled felsic and mafic magmas with an evolution from a significant component of crustal melting toward more mafic composition, a trend that is common in post-orogenic magmas (Bonin, 2004).

Whether these features are characteristic of syn-extension plutons in post-orogenic back-arc environments is the question we address in this paper, through a comparison of the Aegean plutons with those of the northern Tyrrhenian Sea and Tuscany, with a focus on Elba Island in the Tuscan archipelago (figure 3). Striking similarities can indeed be observed between the two contexts in terms of tectonic and magmatic evolution. A similar evolution is observed on the Aegean plutons and those of the Tyrrhenian Sea, and we propose a scenario of formation and emplacement of plutons in a back-arc post-orogenic context below crustal-scale detachments.

2. Geodynamic context

The Aegean and North Tyrrhenian granitoids were emplaced during the Miocene and part of the early Pliocene in the back-arc regions of the Hellenic and Apennines subduction, respectively (Serri et al., 1993; Jolivet et al., 1998; Pe-Piper and Piper, 2002, 2007; Avanzinelli et al., 2009; Jolivet et al., 2015; Rabillard et al., 2018) (Figure 2, Figure 3). These two subduction zones started to retreat approximately at the same time, 30-35 Ma ago (Jolivet and Faccenna, 2000). A first-order change in the geodynamics of this region indeed occurred at this period, also coeval with the hard collision between Africa and Eurasia in the eastern and westernmost Mediterranean. The subducting African lithosphere, locked between two collision zones, continued to subduct northward but with a significant component of retreat. Since that time subduction has been continuous, with however several episodes of slab detachment and tearing (Wortel and Spakman, 2000; Spakman and Wortel, 2004; Faccenna and Becker, 2010; Faccenna et al., 2014). Figure 1 shows the present-day situation as well as two stages at 5 and 15 Ma when the Tyrrhenian and Aegean plutons were forming adapted from the detailed reconstructions of from Romagny et al. (2020). Magmatic events are shown with grey triangles (volcanism) and black squares (plutons). The detailed tectonic evolution, the reconstruction method and the link between magmatism and tectonics are described in discussed in Romagny et al. (2020) and Menant et al. (2016). The progressive retreat of subduction zones and foreland fold-and-thrust belts and/or accretionary wedges is shown coeval with crustal thinning and exhumation of metamorphic core complexes. This evolution of the Northern Tyrrhenian region as a back-arc basin within the overriding plate of the retreating Apennine subduction is not however entirely consensual and alternative models exist, which involve different mechanisms, including escape tectonics (Mantovani et al., 2020).

The Aegean plutons studied in this paper were emplaced during the formation of a large tear in the subducting lithosphere between 16 and 8 Ma (Jolivet et al., 2015). The oldest North Tyrrhenian pluton is dated around 7 Ma in Elba (Westerman et al., 2004) and the youngest ones, Pliocene in age (Serri et al., 1993), are currently exploited for geothermal energy in Tuscany (Rossetti et al., 2008; Gola et al., 2017; Rochira et al., 2018). All these plutons contain a significant component of crustal melts and some of them are linked with migmatite domes such as on Naxos, Mykonos and Ikaria (Jansen, 1977; Urai et al., 1990; Denèle et al., 2011; Beaudoin et al., 2015; Vanderhaeghe et al., 2018). Mixing and mingling with mafic magmas are also observed in some of these plutons and the general evolution shows an increase of the mantle component with time.

The geodynamic setting of the Northern Tyrrhenian Sea and Tuscany is debated and the reader is referred to the papers of Mantovani et al. (2020) and Romagny et al. (2020) for opposite views. Since the late 90's two opposite interpretations have been discussed. One school of thought considers a continuum of extension from the Oligocene to the present with an eastward migration of extension in the back-arc region of the retreating Apennine subduction (Keller and Pialli, 1990; Jolivet et al., 1994; Jolivet et al., 1998; Faccenna et al., 2001a; Faccenna et al., 2001b; Brogi et al., 2003; Brogi et al., 2005; Brogi, 2008; Brogi and Liotta, 2008; Brogi, 2020). Extension starts in the early Oligocene between Corsica and Provence and reaches the highest part of the Apennines in the recent period. Extensional basins, controlled by low-angle east-dipping normal faults migrate eastward following the migration of the magmatic arc. A part of this extension is also accommodated by higher-angle normal faults, most of them dipping eastward, leading to a stretching factor of about 2.2 (Moeller et al., 2013; 2014). The Zuccale low-angle normal fault or an east-dipping ductile extensional shear zone bounding the Monte Capanne pluton, both observed in Elba Island, are part of this continuum of extension in the late Miocene and the Pliocene (Keller and Pialli, 1990; Daniel and Jolivet, 1995; Collettini and Holdsworth, 2004). This type of model is challenged by an alternative view where extension is only very recent, not before the Late Miocene or even later in the Tyrrhenian Sea and where several basins on the mainland of Italy are instead interpreted as compressional (Finetti et al., 2001; Bonini and Sani, 2002; Ryan et al., 2021). One of the main data set which is at the root of this debate is the CROP seismic profile crossing the Tyrrhenian, Tuscany and the Apennines (Finetti et al., 2001). Discussions of this alternative can be found more developed in several papers (Brogi et al., 2005; Brogi, 2008; Brogi and Liotta, 2008; Brogi, 2020). We consider that the compressional model cannot account for the first-order features of the northern Tyrrhenian Sea such as the crustal and lithospheric thickness and the geological evolution of Corsica, Elba, Giglio islands and we deliberately place our research in the framework of the migrating extension models.

Most of these plutons are associated with low-angle normal faults (LANF) and shear zones and they were emplaced in the core of MCCs (Faure et al., 1991; Lee and Lister, 1992; Lister and Baldwin, 1993; Daniel and Jolivet, 1995; Jolivet et al., 1998; Rabillard et al., 2018). These LANF and associated ductile shear zones (we use the term "detachment" for the whole structure, brittle and ductile) started to form before the emplacement of the plutons, in both regions. The main differences between the two regions are the kinematics of these detachments (figures 2 & 3) (Jolivet et al., 2008) and the role of tectonic inheritance. In the Aegean, most of the MCCs are capped by north-dipping detachments except in the southwest where south-dipping detachments are observed. The north-dipping detachments probably partly reactivate former thrusts related to the building of the Hellenides orogenic wedge. Whatever the nature (i.e. reactivated structure or not) and the sense of shear of the Aegean detachments, the interaction with the plutons follows a similar pattern that we recall below (see Rabillard et al., 2018, for details). In the Northern Tyrrhenian Sea and in Tuscany, all detachments dip eastward, i.e. toward the subduction zone. In that case, the detachments cannot reactivate the former thrusts of the internal Apennines that dip westward. Only in the case of the oldest detachments, found in Alpine Corsica, can they correspond to reactivated thrusts. The case of Elba Island shows very well the detachments cutting down-section eastward within the stack of former nappes (Keller and Pialli, 1990; Collettini and Holdsworth, 2004).

The emplacement of plutons underneath extensional detachments may also be influenced by transfer faults accommodating along-strike variations of the rate of extension. This has been mainly discussed for geothermal reservoirs associated with plutons at the intersection of a detachment and a transfer fault, which leads to enhanced permeability and more efficient advection of fluids toward the Earth surface (Dini et al., 2008; Faulds et al., 2009; Liotta et al., 2015; Gola et al., 2017; Roche et al., 2018a; 2018b; Brogi et al., 2021; Liotta et al., 2021). In the case of the Tuscan Archipelago and Tuscany, this possibility has been documented by field studies in eastern Elba and the Gavorrano pluton (Liotta et al., 2015; 2021). The present paper is however mainly focused on the extensional component of deformation and the interactions between low-angle detachments and the emplacement of plutons.

3. Aegean plutons

We first recall the main findings of the interactions between detachments and plutons as documented from the Aegean. The Miocene Aegean and Menderes plutons were emplaced during a short time period between ~20 Ma and 8 Ma, the oldest cropping out in the Menderes massif and the youngest in the western part of the Aegean region (figure 2) (Jolivet et al., 2015). Those occupying the Cycladic domain are all associated with detachments, either north or south-dipping (figure 2) (Grasemann and Petrakakis, 2007; Rabillard et al., 2018). Except for Serifos and Lavrion plutons, associated with the West Cycladic Detachment System (WCDS)

(Grasemann and Petrakakis, 2007; Berger et al., 2013; Scheffer et al., 2016), the plutons crop out in the core of MCCs exhumed by north-dipping detachments, such as the North Cycladic Detachment System (NCDS) (Gautier and Brun, 1994b, a; Jolivet et al., 2010) or the Naxos-Paros Fault System (NPFS) (Urai et al., 1990; Gautier et al., 1993; Vanderhaeghe, 2004; Bargnesi et al., 2013; Cao et al., 2017). The detachment upper plate is made of the Upper Cycladic Nappe, a remnant of the Pelagonian domain, made of greenschists-facies metabasites or serpentinite with, in a few cases, early to late Miocene sediments deposited during extension (Angelier et al., 1978; Sanchez-Gomez et al., 2002; Kuhlemann et al., 2004; Menant et al., 2013). The MCCs are made of various units of the Cycladic Blueschists, more or less retrograded in the greenschist-facies, or the Cycladic basement, showing H*T*-L*P* metamorphic facies and even anatectic conditions on several islands, such as Naxos, Paros, Mykonos or Ikaria (Buick and Holland, 1989; Urai et al., 1990; Buick, 1991; Keay et al., 2001; Duchêne et al., 2006; Seward et al., 2009; Kruckenberg et al., 2011; Beaudoin et al., 2015; Laurent et al., 2015; Rabillard et al., 2015; 2018). The plutons intruded these MCCs and were sheared at the top by the detachments during their emplacement (Rabillard et al., 2018).

The granitoids show a variety of facies and composition, but most of them have a crustal melting component and some are closely associated with migmatites, as on Ikaria or Mykonos (Denèle et al., 2011; Beaudoin et al., 2015). Compositions show a common trend for these plutons indicating that they crystallized primarily from I-type magmas with some contamination by the continental crust and little fractionation (figure A1, Appendix A). Field evidence show a close association of these I-type intrusions with two-micas granites (in Ikaria for instance), migmatites, or both (Ikaria, Naxos, Paros, Rheneia-Delos) (Pe-Piper et al., 1997; Pe-Piper, 2000; Pe-Piper et al., 2002; Vanderhaeghe, 2004; Bolhar et al., 2010; Bolhar et al., 2012; Bargnesi et al., 2013; Beaudoin et al., 2015; Laurent et al., 2015; Jolivet et al., 2021). Tinos, Ikaria and Serifos granitoids were emplaced in several magma batches with an evolution through time, characterized by more and more mafic compositions and a decrease of the grain size (Grasemann and Petrakakis, 2007; Ring, 2007; Bolhar et al., 2010; Petrakakis et al., 2010; de Saint Blanquat et al., 2011; Bolhar et al., 2012; Beaudoin et al., 2015; Laurent et al., 2015; Rabillard et al., 2015; Ducoux et al., 2016). On Serifos and Naxos, the farthest parts of the pluton from the detachment show an enrichment in mafic enclaves and evidence for magma mixing and mingling in the roots of the rising plutons (Rabillard et al., 2015; Bessière et al., 2017; Rabillard et al., 2018).

A common evolution is observed in several of these plutons during their interaction with the system of detachments exhuming their host MCC (Rabillard et al., 2018). A series of two or three detachments is observed (figure 5, figure 6). The deepest one is mostly ductile and has started to act long before the granitic intrusion that ultimately intrudes it. The upper detachments are mostly brittle and are locally intruded by dykes and sills emanating from the main pluton. When a sedimentary basin is present, it is deposited on top of the uppermost detachment during extension and can be partly affected by mineralized veins (Menant et al., 2013). All plutons show a gradient of shearing deformation toward the detachment with an evolution from ductile to brittle (Figure 5). The maps shown in figure 5 were drawn after detailed field observations and the construction of a scale of up to 7 grades of progressive deformation, from non-deformed granitic texture to ultra-mylonites, with the progressive appearance of foliation, stretching lineation, localization of C and C' shear bands (Berthé et al., 1979; Lister and Snoke, 1984), for details see Rabillard et al. (2018). The inner parts of the plutons show mixing of acidic and mafic magmas and a co-magmatic deformation co-axial with the post-solidus deformation along the detachment (Rabillard et al., 2015; 2018). The flow of magma is thus oriented by the regional strain field. Serifos shows (i) a decrease of grain size through time with an inner facies with smaller grain size and finally fine-grained dykes and (ii) evidence for hydrothermalism in the root zone of the pluton, suggesting that the magmatic system was open upward with a possible volcano-plutonic system (Rabillard et al., 2015; 2018).

4. North Tyrrhenian plutons

We now describe our observations in the Monte Capanne pluton on Elba Island and replace them in the regional tectonic context. The Monte Capanne pluton (figure 7) is the oldest of a series of plutons cropping out in the Tuscan archipelago and onshore Tuscany (Serri et al., 1993; Westerman et al., 2004; Avanzinelli et al., 2009). Among the youngest plutons are those powering the active geothermal fields of Larderello and Monte Amiata (Camelli et al., 1993; Brogi et al., 2003; Rossetti et al., 2008). These plutons belong to magmas migrating from west to east between the end of the Oligocene and the Quaternary, mimicking the migration of the Apennines thrust system and the HP-LT metamorphism of the internal Apennines and Tuscan Archipelago which started earlier at the end of Oligocene (Serri et al., 1993; Jolivet et al., 1998) (figure 3). This situation is thus very similar to the Aegean Sea. The decrease of the time lag between the recording of H*P*-L*T* metamorphism or the activation age of the thrust front and the magmatism has been interpreted as a consequence of slab steepening during retreat (Jolivet et al., 1998; Brunet et al., 2000). Magmatism is recorded in the Tuscan archipelago (Capraia, Elba, Giglio islands) from 8 to 5 Ma with plutons in Elba and Giglio and volcanism in Capraia, and the mantle source of the magma appears highly contaminated by subduction-related and crustal-derived metasomatic fluids (Gagnevin et al., 2011).

Pluton ages decrease eastward from ~8 Ma to 2-3 Ma (figure 3). The oldest plutons are observed offshore on Elba (Monte Capanne and Porto Azzuro plutons), Monte Cristo and Giglio islands (Westerman et al., 1993) (figure 3). These four plutons are granodiorites/monzogranites and they all display a contamination with crustal magmas with a main source thought to be lower crustal anatexis (Serri et al., 1993; Innocenti et al., 1997). They were emplaced within an overall extensional context during the rifting of the Northern Tyrrhenian Sea in the back-arc region of the Apennines (Jolivet et al., 1998). First evidenced in Alpine Corsica and on Elba island, a series of east-dipping low-angle detachments controlled the kinematics of extension along the Corsica-Apennines transect from the Oligocene onward (Jolivet et al., 1998). Extension is shown to migrate from west to east with time and it is active at present in the highest altitude regions of the Apennines just west of Corno Grande peak with however west-dipping normal faults (D'Agostino et al., 1998). The youngest east-dipping low-angle normal faults are seismically active in the Alto Tiberina region (Collettini and Barchi, 2002, 2004; Pauselli and Ranalli, 2017). Evidence for top-to-the east shearing deformation is found within the plutons of the Tuscan archipelago, but the detachments crop out nicely mostly on Elba island (Keller and Pialli, 1990; Daniel and Jolivet, 1995; Collettini and Holdsworth, 2004; Liotta et al., 2015).

However, another vision that stems from different interpretations of the observed top-the east shear zones in eastern Elba in the vicinity of the Zuccale Detachment, is proposed for the emplacement of those plutons. Detailed studies have documented the progressive deformation along these shear zones from brittle to ductile and the HT-LP conditions associated with the most ductile ones and they have been dated from the Pliocene (Mazzarini et al., 2011; Musumeci and Vaselli, 2012; Musumeci et al., 2015; Massa et al., 2017; Papeschi et al., 2017, 2018; Viola et al., 2018; Papeschi et al., 2019). Their interpretation can then be debated. They can either be west-dipping thrusts or back-tilted top-to-the east extensional ductile shear zones coeval with the progressive localization of the Zuccale Detachment, which is our interpretation following Daniel and Jolivet (1995).

4.1. Monte Capanne pluton, Elba Island

Elba, the largest island of the Tuscan archipelago, shows the relations between peraluminous magmatic bodies and two east-dipping low-angle shear zones cutting down-section within the Tuscan nappe stack emplaced before extension started (figure 7) (Keller and Pialli, 1990; Bouillin et al., 1993; Pertusati et al., 1993; Daniel and Jolivet, 1995; Westerman et al., 2004; Bianco et al., 2015). Five thrust packages (complexes I to V) are separated by west-dipping low-angle reverse faults (Trevisan, 1950; Barberi et al., 1967; Perrin, 1975; Pertusati et al., 1993; Bianco et al., 2015; Bianco et al., 2019). Long thought free of any H*P*-L*T* imprint, at variance with the nearby Gorgona and Giglio islands, the nappe stack has recently revealed H*P*-L*T* parageneses along the east coast of the island (Bianco et al., 2015). Through a correlation with the H*P*-L*T* units of Gorgona (Rossetti et al., 1999), where ^{40}Ar/^{39}Ar dating on micas yielded ages around 25 Ma (Brunet et al., 2000), the Elba blueschists were attributed to the Late Oligocene and Early Miocene, which was recently confirmed with ^{40}Ar/^{39}Ar ages around 20 Ma (Bianco et al., 2019).

The Nappe stack is intruded by the shallow-level San Martino and Portoferraio porphyries coeval with the Monte Capanne pluton (figure 7), spanning a short period between 8 and 6.8 Ma, showing that the magma has intruded the detachment in a late stage (Saupé et al., 1982; Juteau et al., 1984; Ferrara and Tonarini, 1985; Bouillin et al., 1994; Westerman et al., 2004). The Monte Capanne intrusion makes the major part of the western half of the island and the highest peak. It is surrounded by a contact metamorphic aureole developed at the expense of the nappe stack (Duranti et al., 1992; Dini et al., 2002; Rossetti et al., 2007; Rossetti and Tecce, 2008). The metamorphic parageneses within the aureole suggest an emplacement at a depth of 4-5 km (Dini et al., 2002; Rocchi et al., 2002; Farina et al., 2010; Pandeli et al., 2018). The pluton shows an internal deformation with a gradient of shearing toward the east attested by the magnetic fabric, stretching lineation and sense of shear (Bouillin et al., 1993; Daniel and Jolivet, 1995). The pluton and the metamorphic aureole are separated from the nappe stack by an east-dipping low-angle shear zone (Capanne shear zone) evolving into a brittle east-dipping fault (eastern border fault) (Daniel and Jolivet, 1995). Syn-kinematic contact metamorphism minerals coeval with top-to-the east kinematic indicators attest for the syn-kinematic nature of the intrusion (Daniel and Jolivet, 1995; Pandeli et al., 2018).

The eastern part of the island shows granitic dykes emanating from the buried younger Porto Azzuro pluton intruding the Calamiti schists complex (Complex I, figure 7) (Daniel and Jolivet, 1995; Maineri et al., 2003; Musumeci and Vaselli, 2012). Here too, evidence for top-to-the east shearing at the time of intrusion have been described (Daniel and Jolivet, 1995) (figure 8). The pluton and the Calamiti schists are topped by the Zuccale low-angle normal fault that cuts down-section across the entire nappe stack with clear evidence of top-to-the east shearing (figure 9) (Keller and Pialli, 1990; Keller et al., 1994; Collettini and Holdsworth, 2004).

The main facies of the Monte Capanne pluton exhibits a constant, peraluminous, monzogranitic composition (Poli et al., 1989; Dini et al., 2002; Gagnevin et al., 2004) while the mafic microgranular enclaves (MME) varies from tonalitic-granodioritic to monzogranitic. The leucogranitic dykes are syenogranitic in composition (Gagnevin et al., 2004). Gagnevin et al. (2004) proposed a multiphase magmatic emplacement from peraluminous magmas issued from melting of a metasedimentary basement and hybridized with mantle-derived mafic magmas whose heat supply possibly enhanced wall-rock assimilation. In addition, injection of mantle-derived magma in the Sant' Andreas facies would have triggered extensive fractionation and mixing of the basic magma with the resident monzogranitic mush (Poli and Tommasini, 1991).

The internal magmatic structure of Monte Capanne pluton has been described based on the abundance of large alkali-feldspar phenocrysts (Farina et al., 2010). Three main facies corresponding to different magma batches emplaced within a too short period to be discriminated according to geochronology are reported with downward fining of grain size (figure 7). The largest grain size characterizes the upper Sant' Andrea facies that mainly crops out in the northwest of the pluton, while the finest grain size is observed in the lower San Piero facies cropping out mainly in its eastern part within the zone affected by the most intense shearing. These three facies delineate an asymmetric dome-shaped bulk structure compatible with the general top-to-the east sense of shear. In the westernmost part of the Monte Capanne pluton near Sant' Andrea mafic products are observed as large enclaves, with evidence of magma mixing and mingling. These mafic enclaves are mostly found in the Sant' Andrea facies that was emplaced first. Their occurrence in the westernmost part of the plutonic body, the farthest from the detachment, with a geometry similar to what is observed on Serifos island in the Cyclades, suggests that they are associated with the root of the pluton.

Assuming that the three main felsic facies correspond to three successive intrusion batches, one observes an evolution toward finer grain size through time, an evolution that is compatible with progressive exhumation and also with a shorter residence time in the magma chamber, suggesting opening of the magmatic plumbing toward the surface leading to volcanic activity, as recorded above the detachment. The last episodes of intrusive activity are seen as a series of felsic dykes striking N-S or NE-SW, due to eastward extensional brittle deformation while the pluton was at near solidus conditions.

4.2. Orientation of K-feldpar megacrysts

We conducted a detailed study of the orientation of feldspar megacrysts along the shore near Sant'Andrea (figures 10, 11, 12). The pluton is there characterized by a high concentration of megacrysts and of mafic enclaves reaching several meters in size. Megacrysts show euhedral shapes in general. Although the orientation of megacrysts is quite stable at the scale of a few hundred meters, in the westernmost region the presence of the large enclaves is associated with a disorientation of the megacrysts (figure 11A), indicating increasing tortuosity of the flow wrapping around them associated with local turbulence in pressure shadows. Smaller enclaves are in general aligned with the megacrysts. Some of the mafic enclaves with lobate shapes show a sharp boundary with the felsic matrix, suggesting quenching of a hot mafic magma within the cooler felsic magma (Fernandez and Barbarin, 1991; van der Laan and Wyllie, 1993; Fernandez and Gasquet, 1994). Other enclaves are less mafic and show evidence of magma mingling-mixing. The disaggregation process of the mafic magma responsible of theses enclaves could happened either in a deep-seated magmatic chamber (Christofides et al., 2007), or more likely in the ascent conduit as a result of remelting of chilled mafic margins (Fernández and Castro, 2018) and subsequent viscous fingering dynamics (Perugini et al., 2005). Megacrysts contain inclusions of biotite, plagioclase and quartz and show euhedral shapes in general, although resorption surface has been noticed (Gagnevin et al., 2008). Other enclaves are less mafic and show evidence of magma mingling-mixing. These enclaves are associated with an aureole where feldspar crystals are concentrated, showing that the assimilation of the enclave occurred at the magmatic stage. Megacrysts are sometimes included within the mafic enclaves, showing that they were already present before the solidification of enclaves and thus providing evidence of low viscosity contrast between the enclaves and the host magma at the magmatic stage. All these observations suggest that this western zone is a mixing between a mafic magma of mantle origin and a felsic magma partly issued from crustal anatexy and that this part of the pluton is close to the main feeder. This conclusion is confirmed by AMS (anisotropy of magnetic susceptibility) showing that the magnetic foliation and lineation are steeper there than anywhere else in the pluton (Bouillin et al., 1993).

Further to the east, still within the Sant' Andrea facies, the main granite is intruded by a N-S syeno-granitic dyke-like structure near Cotoncello headland, made of a finer-grained facies and a lower concentration of megacrysts and enclaves (figure 8D, figure 10). In its vicinity, the host granite contains folded schlierens with cross-bedding (Figure 10A). Within these large schlierens, the megacrysts are aligned parallel with the folded foliation of biotite-rich layers.

From place to place, decametric megacryst-rich mush zones enriched in decametric and rounded mafic enclaves occur in this host facies (Figure 10B). In addition, isolated blobs of mush, characterized by an irregular shape, are observed in the coarse-grained, megacryst-poor domains (Figure 10C). These blobs originate from the disruption of preexisting mush zones within the root zone by subsequent magma injection as illustrated by a dyke-like structure (Rodríguez and Castro, 2019). This structure is composed of three successive injections characterized by undulating and fuzzy boundaries (Figure 10D). The westernmost injection (injection Ia, figure 10D) shows folded alternating leucocratic flow-sorted layers made of quartz, K-feldspar and plagioclase with more melanocratic layers rich in biotite that can be described as schlierens (Figure 10E). These schlierens are folded and cross-cut by a subsequent and final injection (Figure 10D, injection II). In the easternmost injection (Figure 10D, injection Ib), K-feldspar megacrysts are accumulated and their orientation defines a concave upwards foliation. Such mineral fabric is similar to those described by Rocher et al. (2018) in finger-and-drip structures developed at the margins of the Asha pluton (NW Argentina) and interpreted as mechanical accumulation in a downward localized multiphase magmatic flow. In addition, this megacrysts accumulation is associated at its top with ring schlieren that could represent a cross-section of a schlieren tube (e.g. Žák and Klomínský, 2007) (figure 10F). Ring schlierens are also associated with drip structures in the Asha pluton among others (Paterson, 2009; Rocher et al., 2018). The most external rim between the host body H and injection Ia (Figure 10D) is associated with a reaction zone with recrystallization of quartz and K-felspar (Figure 10E, white arrow). Outside the injections, the mineral fabric shown by the K-feldspar megacrysts tends to reorientate parallel to the rims. All these observations point out to an injection of a low viscosity, crystal poor, magma with a viscosity contrast of about one order of magnitude lower with respect to its host magma (Wiebe et al., 2017). Mineral fabrics and accumulation, folded and ring schlieren indicate that the structures were formed by localized multiphase magmatic flow when the crystallizing host magma remained partially molten, probably containing around 50% of crystals (Weinberg et al., 2001). The Cotoncello dyke-like structure is thus co-magmatic with the Sant'Andrea facies, but the pluton was already enough crystallized to allow the formation of N-S cracks in the crystal mush capable of transmitting tectonic stress where the magma was injected.

Between the Cotoncello dyke and the root zone to the west, the proportion of enclaves and megacrysts is everywhere high. Systematic measurements of felspar megacrysts were made (figure 12). Mineral foliation and lineation represents the main orientation distributions of the orientation of (010) faces and [001] major axis of the measured crystals, respectively. At the scale of a few hundred meters the fabric shows a consistent pattern with a low-angle north-dipping foliation more prominent in regions poorer in mafic enclaves. The lineation is in average E-W trending. Late mafic and acidic dykes strike perpendicular to the lineation. Within the mélange zone the mineral fabric is often perturbated approaching enclave swarms. Then, the fabric becomes more uniform with variations around an average ENE-WSW trend from N30 to N100°E for the long axes of megacrysts.

As the megacrysts were formed in early magmatic conditions (Vernon, 1986; Vernon and Paterson, 2008), they were in suspension within the melt. Such a preferential orientation is due to a rigid rotation of isolated crystals within a viscous matrix submitted to magmatic flow (Fernandez and Laporte, 1984). In the present case, the various observations attesting for a co-magmatic fabric show that the preferential orientation of the megacrysts foliation results from fossilization of the magmatic flow. The large-scale variations of the foliation attitude suggest in addition that the E-W to ENE-WSW flow was laminar in general, except in the immediate vicinity of the large enclaves where the flow wrapping around these stronger bodies was more turbulent.

These detailed observations show that the internal magmatic fabric of the pluton is similar in orientation with its overall tectonic fabric, including the sub-solidus deformation along the eastern margin due to the detachment with a main stretching direction oriented WNW-ESE, as shown by magnetic susceptibility studies (Bouillin et al., 1993) and deformation features near the main eastern contact within the eastern extensional shear zone (Daniel and Jolivet, 1995). This focussing of the pluton fabric, from the magmatic stage to the brittle stage around an E-W stretching direction compatible with the extensional shear along the main detachment, suggests that the magmatic flow was oriented parallel to the main direction of extension active at crustal scale since the magmatic stage. A continuum is thus observed from the magmatic stage to the sub-solidus deformation and the localization of the detachment, and this continues during the emplacement of the younger Porto-Azzuro pluton and the formation of the Zuccale low-angle normal fault.

5. Discussion and modelling

5.1. Synthesis of observations

The coaxiality of the structures measured in the Monte Capanne pluton from its magmatic stage to the tectonic overprint is similar to observations made on the Cycladic plutons, especially Ikaria and Serifos where a similar gradual transition is observed from the magmatic stage to the localisation of strain along the main detachment. The similarity goes further as the root of the pluton shows a mixture of mafic and felsic facies. On Serifos (figure 5), field observations show that the root of the pluton is characterized by vertical or steep dykes and some of them are dilacerated by the top-south flow while the magma is still viscous (Rabillard et al., 2015). Moving toward the detachment, the sub-solidus deformation takes over with a N-S trending stretching lineation and top-south kinematic indicators. A similar evolution can be observed in the Raches pluton of Ikaria island in the Cyclades (Laurent et al., 2015). Emplaced below to top-to-the north detachment, the magma shows a steep foliation in the south far from the detachment and it flattens toward the north to become parallel to the detachment plane. Evidence of co-magmatic stretching and shearing parallel to the regional stretching direction is observed in the southern side of the pluton and sub-solidus mylonitization and ultra-mylonites on the northern side. A similar situation can be described in the case of the Naxos granodiorite (Bessière et al., 2017). All cases show the syn-kinematic character of the pluton, the best evidence being the syn-kinematic contact metamorphism.

The Monte Capanne pluton thus shows clear similarities with the Aegean plutons. Figure 13 shows a simplified scheme of the geometrical and kinematic relations between detachments and plutons based on the examples of the Aegean and the Northern Tyrrhenian, modified from Rabillard et al. (2018). The root zone of the pluton, characterized with an association of mafic and acidic magmas, shows a steeper upward magmatic flow and evidence of co-magmatic stretching and shearing parallel to the regional direction of extension with a kinematics similar to that of the main detachments. During the emplacement of the pluton, the magma chamber progressively opens toward the surface and the granitoids evolve toward finer-grained facies. Progressive extension and exhumation are accompanied by the inflation of the pluton and injection of dykes across the ductile detachment. New detachments are formed above sequentially.

At the scale of Elba Island, the sequential intrusion of the Capanne Pluton and the Porto Azzuro pluton associated with the sequential formation of the Capanne Shear Zone followed by the Zuccale Fault is reminiscent of the migration of detachments within the NCDS and the WCDS, where the last increment of extension being accommodated by a low-angle brittle detachment, the Mykonos Detachment in the case of the NCDS and the Kavos Kyklopas

Detachment in the case of the WCDS. This is another significant similarity between the Aegean and Tyrrhenian plutons.

5.2. *A conceptual model based on published numerical experiments*

This evolution can be compared with numerical models. Thompson and Connolly (1995) summarize the three ways of melting lower continental crust as (1) supplying water to the crust to lower the solidus, (2) decreasing pressure and (3) providing additional heat to the lower crust. They also state that extension alone of a thickened crust is unlikely to reach the conditions of lower crustal melting unless some additional heat is given by the mantle. Back-arc regions above retreating slabs, where the lithosphere is thinned and the asthenosphere advected upward underneath the crust seem to the first order to fit these conditions.

Schubert et al. (2013) have explored numerically the effect of the injection of molten mafic material in an extending crust. They show that the injection of this hot material in the lower crust will induce melting and trigger the formation of felsic magmas that will then ascent along steep normal faults all the way to the upper crust, forming the observed plutons. This is a situation that can easily be compared with the Aegean or the Tuscan archipelago where the granitoids are associated in their root zones with coeval mafic magmas and the felsic plutons ascend along low-angle detachments. In figure 14, we propose a further conceptual model based on numerical experiments of post-orogenic extensional deformation with low-angle shear zones (Huet et al., 2011). In this series of numerical experiments, the thermal gradient and Moho temperature were varied as well as the rheological stratification with either a classical rheological stratification or an inverted crustal structure resulting from the formation of the pre-extension nappe stack, the latter setup being used in figure 14, see also Labrousse et al. (2016) for more details on the dynamics of this system with inverted rheological profiles. This latter choice is designed to mimic the Aegean orogenic wedge where the Cycladic Blueschists Unit is sandwiched between the Cycladic Basement and the Upper Cycladic Unit (UCU) (Huet et al., 2009; Jolivet and Brun, 2010; Ring et al., 2010). The UCU belongs to the Pelagonian paleogeographic domain and is largely composed of an ophiolite, denser and stronger than the CBU (Labrousse et al., 2016) as well as other basement lithologies (Reinecke et al., 1982; Katzir et al., 1996; Soukis and Papanikolaou, 2004; Martha et al., 2016; Lamont et al., 2020). Asymmetric lateral boundary conditions are applied with 1 cm/yr on the left side and no displacement of the right side as in Tirel et al. (2004). The upper surface is free and the base is driven by hydrostatic forces. No prescribed discontinuity is introduced in the model, strain localization is only due to the use of random noise in the cohesion value of the upper crust (for more details, see Huet et al., 2011). The results shown here represent a case where the rheological stratification is inverted and the thermal gradient is high, a likely situation in the Aegean or Tyrrhenian post-orogenic and back-arc contexts.

The conceptual model of the interactions between the numerical model dynamics and the intrusions is that we assume that a batch of mafic magmas, issued from partial melting of the mantle, is injected at the base of the lower crust where it triggers the melting of felsic materials. This leads to the formation of migmatites and collection of the felsic melts in a rising pluton progressively caught in the detachment dynamics as it reaches the upper parts of the crust. The felsic magma is thus deformed while it is still partly liquid and then mylonitized once it has cooled down below the solidus. While extension proceeds, the overburden is removed by the activity of the detachment and the molten material that comes next is injected in lower pressure conditions and finds a faster access to the surface because of extension, thus leading to smaller grainsize plutonic facies and probable volcanism at the surface. While the system of detachments migrates toward the right and a new dome forms, the same situation can be reproduced and a new pluton is emplaced below a detachment further to the right, closer to the active detachment. This evolution is reminiscent of the evolution of Elba Island with the formation of the Monte Capanne pluton in a first stage and the Porto Azzuro pluton in a later stage.

5.3. Testing the concept with a new numerical experiment

Quantitative data on the depth of intrusion of the Monte Capanne pluton can be obtained through the analysis of the metamorphic parageneses in the contact aureole and also assessed by comparison with the nearby Porto Azzurro pluton or the active geothermal field of Larderello. The Porto Azzurro pluton, more recent, induced the formation of a high-temperature contact metamorphism in the Calamiti Schists cropping out underneath the Zuccale Fault. Estimations of the P-T conditions of this metamorphism suggest that the pluton was emplaced at a similar depth of about 6.5 km and the maximum temperature recorded in the schists is about 650°C fringing the muscovite breakdown reaction (Caggianelli et al., 2018). Analysis of the metamorphic aureole also reveals multiple hydrofracturing episode by boron-rich fluids which can be compared to the present-day fluid circulation at depth in the Larderello geothermal field

(Dini et al., 2008). Thermal modelling of an intrusion rising in the upper crust (Rochira et al., 2018) allows constraining the size of the pluton to produce the observed thermal anomaly beneath Larderello, but such model does not allow testing the interactions between the detachment and the rising and cooling pluton. Although evidence of the involvement of transfer faults have been described in the case of the Porto Azzurro pluton (Spiess et al., 2021) we do not address these in our modelling procedure as our model is kept 2-D for the moment.

The conceptual model described above is now tested with new numerical experiments involving the emplacement of magmas like in Schubert et al. (2013), but in a different situation where low-angle detachments form, to see whether the introduction of a low-viscosity material in the model developed by Huet et al. (2011) would drastically change the system dynamics or not. This has been done for figures 15, 16 and 17. The kinematics of exhumation produced by the nappe stacking experiments of Huet et al. (2011) produces extension along long-lived detachment better resembling Mediterranean example than diapiric spreading models that are produced by models with no intermediate weak layers as in Tirel et al. (2004, 2008) or Rey et al. (2009). Hence, in order to test how molten rocks interacts with detachments, we decided to build on our experience and start from this set up which is a 210 km wide model domain submitted to 1cm/yr of extension on its left side for 10 Myr or more with an initial lithospheric column constituted from 25 km upper crust, 10 km weak middle crust, 15 km thick lower crust overlying 40 km of lithospheric mantle. The Moho located at 50 km depth is initially at a temperature of 830°C. We have taken the same rheological parameters which are reported in Table A1 (Appendix A). The four major differences with Huet et al. (2011) are :

i) Erosion and sedimentation applied on the top boundary,
ii) the deforming Wrinkler foundation at the LAB has been replaced by inflow of asthenospheric material with higher thermal diffusivity to simulate small scale convection and keep the base of the lithosphere at 1300°C during the experiments as it was the case in Huet et al. (2011) study,
iii) the numerical code used in this study is pTatin2d (May et al., 2014, 2015) that solves the same momentum equation

$$\nabla.\sigma = \rho g$$

For velocity v, as well as heat conservation

$$-\nabla.(-\kappa\nabla T + vT) + H = \frac{\partial T}{\partial t}$$

for Temperature T as Huet et al. (2011). However, it uses an incompressible visco-plastic rheology minimizing the stress between a dislocation creep regime and Drucker Prager failure

$$\nabla . v = 0$$
$$\sigma = min\left(\sin\phi + 2\ C\cos\phi\ , \dot{\varepsilon}^{\frac{1}{n}} A^{\frac{-1}{n}} e^{\frac{Q+VP}{nRT}}\right)$$

to evaluate an effective viscosity :

$$\eta_r = \frac{\sigma}{2\dot{\varepsilon}}.$$

instead of visco-elasto-plastic rheology based on dislocation creep and Mohr Coulomb failure criteria.

iv) We added a simplified parametrization in order to account for the mechanical effect of a melt in the simulations. The melt fraction M_f has been introduced as a linear function of solidus (T_s) and liquidus (T_l) temperature

$$M_f = \min\left(max\left(\frac{T - T_s}{T_l - T_s}, 0\right), 1\right)$$

following Gerya and Yuen (2003). Based on melt fraction, the density and viscosity of passive markers are modified following algebraic averaging for density

$$\rho = M_f \rho_m + \left(1 - M_f\right)\rho_r,$$

and harmonic averaging for viscosity

$$\eta = \left(\frac{M_f}{\eta_m} + \frac{1-M_f}{\eta_r}\right)^{-1}.$$

The solidus dependence on pressure P (in GPa) is implemented following wet granite solidus of Miller et al. (2003), but we also added a variable temperature offset ΔT to account for more mafic granitic composition as follows:

$$T_s^c = 590 + \frac{250}{10(P+0.1)} + \Delta T$$

and the dependence of liquidus to pressure is modeled following:

$$T_l^c = T_s^c|_{P=0} + 10 + 200P.$$

The mantle is also allowed to melt following Hirshmann et al. (2000) solidus law

$$T_s^m = -5.904P^2 + 139.44P + 1108.08$$
$$T_l^m = T_s^m + 600$$

All solidus and liquidus are represented on figure A2 (Appendix A) as a function of pressure and temperature. For low melting temperature of the lower crust (wet granite solidus with ΔT up to 100°C), the crust is largely molten in the initial conditions and buoyancy effects dominate forming “spreading domes” in the classification of Huet et al. (2011), and this despite the presence of a weak middle crustal layer. For higher melting temperature (ΔT from 150°C) melt proportion remains below the 8% melt connectivity threshold described by Rosenberg and Handy (2005) during most of the simulation. We interpret elements with markers that never crossed that critical threshold as migmatites. In that case, melting does not disrupt the typical asymmetric detachment kinematics observed in Elba and in the Cyclades that was well reproduced by Huet et al. (2011) study. In the late stage of deformation, when the lithospheric mantle is sufficiently attenuated by boudinage, the temperature of the lower crust reaches a sufficient temperature to melt more generously, generating plutons which we define as markers with a melt portion greater than 40%.

With a temperature of 950°C at the surface for the liquidus, the molten layer is initially thicker (figure 14) and strain develops into a spreading dome geometry like in the models of Tirel et al. (2004, 2008) or Rey et al. (2009) , with symmetric strain pattern and limited strain localization. Shear is indeed progressively relocalized on newly formed shear zones at the top of newly exhumed hot material at the structure axis. When the temperature of the liquidus is higher, reaching 1000°C in surface conditions (figure 15), the molten layer is initially thinner, the deformation is persistently more localized on a detachment on one edge of the dome structure and the model evolves with a detachment on the side of a dome with a limited rate of partial melting in the lower crust (<8%). The deformation ultimately migrates to form a second dome where a syn-kinematic low viscosity body develops with a melt ratio >40%, which we interpret as analogue to a granite intrusion. The late evolution of this second dome shows a strongly asymmetric geometry with the shape of the syn-kinematic intrusion controlled by the asymmetry in strain pattern and a low-angle shear zone (figure 16). Figure 17 shows a structural interpretation of the final step of the model for the second dome highlighting this asymmetry: the dome is bounded by two antithetic crustal scale persistent shear zones, with steep and shallow dip, and an eccentricity of the intrusion feeding pipe within the dome. This overall asymmetrical strain and intrusion localization in the case of limited partial melting rate hence reproduces the main features of the strain and intrusion pattern described in the field in the Cyclades and Elba.

Although the model does not show the details of the interactions between the dome and the pluton, which involve percolation of melts, drainage through migmatites and dyke-swarms, and progressive intrusion of the detachment by the rising granite, the overall geometry and kinematics is similar with the natural case. The observed geometry is better reproduced in runs with higher crustal melting temperatures and limited melt production. Low temperature melting reactions for the continental crust are the wet solidus and the muscovite dehydration solidus, while biotite and hornblende dehydration melting reactions could represent higher temperature melting reactions (Weinberg and Hasalová, 2015). The model does not show either the role of mafic injections at the base of the model. In the case of the Aegean and Monte Capanne, we have postulated that mafic melts, generated by partial melting of the mantle in the arc and back-arc region, intrude the lower crust and trigger the generation of felsic melts that then rise within the dome. This is an additional input of heat in the model that would also localize the weakest layers and thus the deformation and likely favor the evolution of the model in the same direction as in the model presented here with a lower melting temperature. Similar evolution can arise with an additional input of water in the lower crust. This water may originate from amphibole-rich gabbros (sanukitoides) that could act as water donors enhancing lower crustal partial melting to further produce secondary I-type granites (Castro, 2020). In the Aegean arc, whereas amphibole bearing, I-type granites (Naxos and Serifos granodiorites among others) likely reassemble secondary I-type granites as described by Castro et al. (2020 and references therein), the origin of this water remains elusive as amphibole-bearing mantle magmas are not yet evidenced in the migmatites.

Castro (2020) pointed out that melting of the lower crust is enhanced by both heat and water supplied by mantle derived mafic magmas. In particular, partial melting of granulitic component triggered by adding water from a mafic, mantle-related, component (vaugnerites) can represent the potential origin of secondary I-type granites as demonstrated by the experimental approach (Castro, 2020). Castro (2020) followed the concept of Chappell & Stephens (1988) whereby the possible dual origin of I-Type magma stems from primary I-type magmas issued from coeval subduction, while secondary I-Type magmas are more likely related to melting of old subduction-related rocks. In the Aegean and Tyrrhenian tectonic settings, there is no evidence so far for the presence in the outcropping migmatitized crust of mafic components such as sanukitoids issued from older subduction-related rocks in sufficient volume to be the main donors of water. In contrast, there are many evidences of mafic mantle-derived magmas, coeval with the I-Type granites *s.l.* described in our study. For example, at the root of the Serifos granodiorite (Aegean Sea), Rabillard et al. (2015) describe mafic dykes disrupted into enclave swarms scattered throughout the whole magmatic body. Injection of mafic hydrous component took place during the whole emplacement period of the pluton that was crosscut by basaltic dykes while the granite was at near-solidus conditions. Closely similar observations can be done in the Tyrrhenian granitoids. For example, the main facies of the Monte Capanne pluton exhibits a constant, peraluminous, monzogranitic composition (Poli and Tommasini, 1991; Dini et al., 2002; Gagnevin et al., 2004) while the mafic microgranular enclaves (MME) varies from tonalitic-granodioritic to monzogranitic. The leucogranitic dykes are syenogranitic in composition (Gagnevin et al., 2004). Gagnevin et al. (2004) proposed a multiphase magmatic emplacement from peraluminous magmas issued from melting of a metasedimentary basement and hybridized with mantle-derived mafic magmas whose heat supply possibly enhanced wall-rock assimilation. In addition, injection of mantle-derived magma in the San't Andrea facies would have triggered extensive fractionation and mixing of the basic magma with the resident monzogranitic mush (Poli and Tommasini, 1991).

We thus fully agree with the assumption of Castro (2020) pointing out that the supply of water to the lower crust is a necessary condition to produce I-type granites, but we believe from the previous petrological studies combined with our field observations that the mafic magmas derived from the coeval mantle are the main donors of water during the partial melting of the lower crust. Distinguishing the two I-Type granites in both Aegean and Tyrrhenian granitoids can be completed by an extensive geochemical study of major and trace elements as illustrated by the synthesis made by Castro (2020) for I-type granites emplaced in different tectonic settings. This approach is not in the scope of our study as the origin of the mafic component has no significant direct impact on the interaction between plutons and detachments faults. Nevertheless, we show basic geochemical diagrams to reinforce the interpretations on lower crust melting and the arrival of mantle-derived magmas at the time of extension and dome formation. In order to illustrate the chemical evolution of I-Type granites in the Aegean and Tyrrhenian settings, a complementary figure is proposed in appendix A (figure A1) issued from a compilation of geochemical analyses. This MgO *vs* SiO2 Harker diagram clearly shows the classical negative correlation found in I-type hornblende-biotite-bearing granites. The microgranular enclaves represents the mafic hydrous melts that reached the upper crust while they mixed/mingled with differentiated melts either during ascent (Fernández and Castro, 2018) or at the base of the magmatic chambers (as well illustrated in Serifos granodiorite by Rabillard et al., 2015). Mixing/migling processes between mafic mantle-derived melts and acid magmas produce composite batholiths (Poli and Tommasini, 1991) as illustrated by the case of the Elba Island magmatic complex shown for comparison (see Dini et al., 2002 for explanation). An additional element should be considered: the asymmetric model of Huet et al. (2011) or the model shown here are relevant situations for entraining surface fluids down into the lower crust (Mezri et al., 2015), while a symmetrical model with a spreading dome would not

The metamorphic parageneses associated with contact metamorphism in the case of Elba suggests a depth of emplacement of the pluton of 4-6 km. In the numerical model, the genesis of the pluton starts in the lower crust at a larger depth. The contact metamorphism observed in the field characterizes the upper part of the pluton after it had risen within the crust, which may explain this apparent contradiction.

One additional factor has not been considered in this study, the heterogeneity of the crust inherited from earlier tectonic events. It has been shown by numerical experiments that dipping heterogeneities in the crust mimicking structures inherited from nappe stacking help localizing deformation, favoring the development of asymmetrical extensional structures and the development of MCCs (Le Pourhiet et al., 2004; Huet et al., 2011; Lecomte et al., 2011; 2012). Using this sort of initial conditions with melting would also favor the localization of deformation on a single detachment. It may alternatively favor the development of several asymmetric domes with low-angle detachments. Future studies should focus on testing such initial conditions and also test these processes in 3-D.

The comparison of the Aegean and North Tyrrhenian plutons shows that the model of interactions between plutons and detachments proposed by Rabillard et al. (2018) is reproducible in similar contexts in different regions and can thus be probably generalized. The comparison of this field-based conceptual model with numerical models moreover suggests that this conceptual model is physically feasible. It requires the concomitance of post-orogenic extension, thus extension set on an orogenic wedge, and a back-arc context to provide the necessary heat and water for the generation of magmas in the mantle and the crust. The possibility of a slab tear would be even more favorable as it increases the possibilities of advecting hot asthenosphere directly below the extending crust.

As shown in the 3-D numerical experiments of Roche et al. (2018), slab retreat and back-arc extension lead to the boudinage of the lithosphere with a spacing of ~100 km which will then localize the formation of crustal domes and detachments. This type of evolution may explain the formation of the lines of domes observed in the Aegean and the Menderes Massif. Whether the boudinage also focuses the collection of mantle-derived magmas below the domes is a question that should be addressed by further modelling. This question is important also because the interactions between plutons and detachments described here and in Rabillard et al. (2018) may provide guides for geothermal exploration. The case of the Menderes Massif is exemplary of the intimate relations between active geothermal fields and crustal-scale detachments (Roche et al., 2018). The case of the Tuscan Archipelago is partly similar with the geothermal fields of Larderello and Monte Amiata developed above recent shallow plutons in a context of asymmetric extension with top-to-the east low-angle shear zones (Jolivet et al., 1998; Brogi et al., 2003; Rochira et al., 2018). The Monte Capanne and Porto Azzuro plutons on Elba are associated with hydrothermal activities and mineralization (Maineri et al., 2003; Rossetti and Tecce, 2008; Liotta et al., 2015) that make them good exhumed analogues of active geothermal fields, a situation that is found also in the Cyclades with the mineralizations observed on Mykonos or Serifos in the Cyclades (Salemink, 1985; St. Seymour et al., 2009; Menant et al., 2013; Tombros et al., 2015; Ducoux et al., 2016).

6. Conclusions

The comparison between the Aegean and Tyrrhenian Miocene plutons shows striking similarities in their interactions with coeval detachments. These plutons were all emplaced underneath low-angle ductile shear zones and brittle detachments in a post-orogenic back-arc environment where extra heat is provided by advected asthenospheric mantle. The roots of those felsic plutons show a mixing with mafic magmas. The magmatic fabric is steep in the vicinity of the roots and shallows toward the detachments. The plutons record substantial stretching and shearing coaxial with the regional deformation while they still contain a significant amount of melt. In sub-solidus conditions, the granitoids are then mylonitized when approaching the detachment, until the formation of ultra-mylonites and pseudotachylytes. In both cases too, the felsic magma intrudes the detachment and invades the upper plate. A migration of detachments is then observed from the deep and ductile detachments to more brittle and surficial ones. Late magmatic batches show a smaller grain size compatible with an opening of the magma chamber toward the surface suggestive of the volcano-plutonic context of these plutons. To account for these similarities suggesting that this model can be generalized we proposed a conceptual model where mafic magmas batches are injected in the lower crust of an extending orogenic wedge in a back-arc region with low-angle detachments. These mafic injections trigger the melting of the lower crustal felsic material and the ascent of felsic plutons in the crust, controlled by the low-angle detachments. The migration of the detachments through time in the model explains the migration of plutons and detachments observed in the Tuscan Archipelago and in Tuscany from the Late Miocene to the Late Pliocene, as well as in the Aegean. This conceptual model is tested with a numerical approach showing the impact of melt supply in the development of the dome strain pattern. The observed asymmetry of strain localization and intrusion are reproduced for a limited melting rate, while a higher melting rate would lead to the development of a completely different dome structure. The geometry and kinematics observed in the field are well reproduced by the model. These intimate interactions between plutons and detachments can be foreseen as useful guides for the prospection and understanding of geothermal and associated mineralization.

Author contribution: Laurent Jolivet, Laurent Arbaret, Florent Cheval-Garabedian, Vincent Roche and Aurélien Rabillard did the field work in the Aegean, Loïc Labrousse and Laetitia Le Pourhiet designed the modeling procedure and ran the numerical experiments. All authors contributed to the writing of the manuscript.

Competing interests: The authors declare that they have no conflict of interest.

Acknowledgments: This paper is a contribution of the ERC Advanced Research Grant RHEOLITH (grant agreement No.290864), of Institut Universitaire de France and Labex VOLTAIRE. The paper benefited from the positive suggestions of Antonio Castro and Andrea Brogi who reviewed the first draft.

References

Angelier, J., Glaçon, G., Muller, C., 1978. Sur la présence et la position tectonique du Miocène inférieur marin dans l'archipel de Naxos (Cyclades, Grèce). C. R. Acad. Sc. Paris 286, 21-24.

Avanzinelli, R., Lustrino, M., Mattei, M., Melluso, L., Conticelli, S., 2009. Potassic and ultrapotassic magmatism in the circum-Tyrrhenian region: Significance of carbonated pelitic vs. pelitic sediment recycling at destructive plate margins. Lithos 113, 213–227; doi:210.1016/j.lithos.2009.1003.1029.

Barberi, F., Giglia, G., Innocenti, F., Marinelli, G., Raggi, G., Ricci, C.A., Squarci, P., Taffi, L., Trevisan, L., 1967. Carta geologica dell' isola d'Elba scala 1:25000. C.N.R. Roma.

Bargnesi, E.A., Stockli, D.F., Mancktelow, N., Soukis, K., 2013. Miocene core complex development and coeval supradetachment basin evolution of Paros, Greece, insights from (U–Th)/He thermochronometry. Tectonophysics 595-596, 165-182, dx.doi.org/110.1016/j.tecto.2012.1007.1015.

Beaudoin, A., Augier, R., Laurent, V., Jolivet, L., Lahfid, A., Bosse, V., Arbaret, L., Rabillard, A., Menant, A., 2015. The Ikaria high-temperature Metamorphic Core Complex (Cyclades, Greece): Geometry, kinematics and thermal structure. Journal of Geodynamics 92, 18-41, http://dx.doi.org/10.1016/j.jog.2015.1009.1004.

Berger, A., Schneider, D.A., Grasemann, B., Stockli, D., 2013. Footwall mineralization during Late Miocene extension along the West Cycladic Detachment System, Lavrion, Greece. Terra Nova 25, 181-191, doi: 110.1111/ter.12016.

Berthé, D., Choukroune, P., Jegouzo, P., 1979. Orthogneiss, mylonite and non coaxial deformation of granites : the example of the South Armorican Shear Zone. J. Struct. Geol. 1, 31-42.

Bessière, E., Rabillard, A., Précigout, J., Arbaret, L., Jolivet, L., Augier, R., Menant, A., Mansard, N., 2017. Strain localization within a syn-tectonic intrusion in a back-arc extensional context: the Naxos monzogranite (Greece). Tectonics 37, DOI: 10.1002/2017TC004801.

Bianco, C., Brogi, A., Caggianelli, A., Giorgetti, G., Liotta, D., Meccheri, M., 2015. HP-LT metamorphism in Elba Island: Implications for the geodynamic evolution of the inner

Northern Apennines (Italy). Journal of Geodynamics 91, 13-25; http://dx.doi.org/10.1016/j.jog.2015.1008.1001.

Bianco, C., Godard, G., Halton, A., Brogi, A., Liotta, D., Caggianelli, A., 2019. The lawsonite-glaucophane blueschists of Elba Island (Italy). Lithos 348-349, 105198; https://doi.org/105110.101016/j.lithos.102019.105198.

Bolhar, R., Ring, U., Allen, C.M., 2010. An integrated zircon geochronological and geochemical investigation into the Miocene plutonic evolution of the Cyclades, Aegean Sea, Greece: Part 1: Geochronology. Contrib Mineral Petrol 160, 719–742, DOI 710.1007/s00410-00010-00504-00414.

Bolhar, R., Ring, U., Kemp, A.I.S., Whitehouse, M.J., Weaver, S.D., Woodhead, J.D., Uysal, I.T., Turnbull, R., 2012. An integrated zircon geochronological and geochemical investigation into the Miocene plutonic evolution of the Cyclades, Aegean Sea, Greece: part 2: geochemistry. Contr. Miner. Petrol. 164, 915-933.

Bonin, B., 2004. Do coeval mafic and felsic magmas in post-collisional to within-plate regimes necessarily imply two contrasting, mantle and crustal, sources? A review. Lithos 78 1–24; doi:10.1016/j.lithos.2004.1004.1042.

Bonini, M., Sani, F., 2002. Extension and compression in the Northern Apennines (Italy) hinterland: Evidence from the late Miocene-Pliocene Siena-Radicofani Basin and relations with basement structures. Tectonics 21, 1010; 1010.1029/2001TC900024.

Bouillin, J.P., Bouchez, J.L., Lespinasse, P., Pêcher, A., 1993. Granite emplacement in an extensional setting: an AMS study of the magmatic structures of Monte Capanne (Elba, Italy). Earth and Planetary Science Letters 118, 263-279.

Bouillin, J.P., Poupeau, G., Sabil, N., 1994. Etude thermo-chronologique de la dénudation du pluton du Monte Capanne (île d'Elbe, Italie) par les traces de fission. Bulletin de la Société Géologique de France 165, 19-25.

Brogi, A., 2008. The structure of the Monte Amiata volcano-geothermal area (Northern Apennines, Italy): Neogene-Quaternary compression versus extension. Int J Earth Sci (Geol Rundsch) 97, 677–703; DOI 610.1007/s00531-00007-00191-00531.

Brogi, A., 2020. Late evolution of the inner Northern Apennines from the structure of the Monti del Chianti-Monte Cetona ridge (Tuscany, Italy). Journal of Structural Geology 141 (2020) 104205; https://doi.org/104210.101016/j.jsg.102020.104205.

Brogi, A., Caggianelli, A., Liotta, D., Zucchi, M., Spina, A., Capezzuoli, E., Casini, A., Buracchi, E., 2021. The Gavorrano Monzogranite (Northern Apennines): An Updated

Review of Host Rock Protoliths, Thermal Metamorphism and Tectonic Setting. Geosciences 11, 124; https:// doi.org/110.3390/geosciences11030124.

Brogi, A., Lazzarotto, A., Liotta, D., Ranalli, G., 2003. Extensional shear zones as imaged by reflection seismic lines: the Larderello geothermal field (central Italy). Tectonophysics 363, 127-139.

Brogi, A., Lazzarotto, A., Liotta, D., Ranalli, G., CROP18 Working Group, 2005. Crustal structures in the geothermal areas of southern Tuscany (Italy): Insights from the CROP 18 deep seismic reflection lines. Journal of Volcanology and Geothermal Research 148, 60–80.

Brogi, A., Liotta, D., 2008. Highly extended terrains, lateral segmentation of the substratum, and basin development: The middle-late Miocene Radicondoli Basin (inner northern Apennines, Italy). Tectonics 27, TC5002, doi:5010.1029/2007TC002188.

Brown, M., 1994. The generation, segregation, ascent and emplacement of granite magma: the migmatite-to-crustally-derived granite connection in thickened orogens. Earth-Science Reviews 36, 83-130.

Brown, M., 2007. Crustal melting and melt extraction, ascent and emplacement in orogens : mechanisms and consequences. J. Geol. Soc London 164, 709-730.

Brown, M., Solar, G.S., 1998. Shear-zone systems and melts: feedback relations and self-organization in erogenic belts. J. Struct. Geol 20, 211-227.

Brunet, C., Monié, P., Jolivet, L., Cadet, J.P., 2000. Migration of compression and extension in the Tyrrhenian Sea, insights from 40Ar/39Ar ages on micas along a transect from Corsica to Tuscany. Tectonophysics 321, 127-155.

Buick, I.S., 1991. The late alpine evolution of an extensional shear zone, Naxos, Greece. J. Geol. Soc. 148, 93-103; doi:110.1144/gsjgs.1148.1141.0093.

Buick, I.S., Holland, T.J.B., 1989. The P-T-t path associated with crustal extension, Naxos, Cyclades, Greece, in: Daly, J.S. (Ed.), Evolution of metamorphic belts, pp. 365-369; doi:310.1144/GSL.SP.1989 .1043.1101.1132.

Caggianelli, A., Zucchi, M., Bianco, C., Brogi, A., Liotta, D., 2018. Estimating P-T metamorphic conditions on the roof of a hidden granitic pluton: an example from the Mt. Calamita promontory (Elba Island, Italy). Ital. J. Geosci. 137, 238-253; https://doi.org/210.3301/IJG.2018.3311.

Camelli, G.M., Dini, I., D, L., 1993. Upper crustal structure of the Larderello geothermal field as a feature of post-collisional extensional tectonics (southern Tuscany, Italy),, ,. Tectonophysics 224, 413-423.

Cao, S., Neubauer, F., Bernroider, M., Genser, J., Liu, J., Friedl, G., 2017. Low-grade retrogression of a high-temperature metamorphic core complex: Naxos, Cyclades, Greece. Geological Society of America Bulletin 129, 93–117, doi:110.1130/B31502.31501.

Castro, A., 2020. The dual origin of I-type granites: The contribution from laboratory experiments, in: Janousek, V., Bonin, B., Collins, W.J., Farina, F., Bowden, P. (Eds.), Post-Archean Granitic Rocks: Petrogenetic Processes and Tectonic Environments.Geol. Soc. London, Spec. Pub., 491 Geological Society of London, London, pp. 101-145; DOI: https://doi.org/110.1144/SP1491-2018-1110.

Chappell, B.W., Stephens, W.E., 1988. Origin of infracrustal (I-type) granite magmas. Transactions of the Royal Society of Edinburgh, Earth Sciences 79, 71–86; https://doi.org/10.1017/S0263593300014139.

Chopra, P.N., Paterson, M.S., 1984. The role of water in the deformation of dunite. J. Geophys. Res 89, 7861-7876.

Christofides, G., Perugini, D., Koroneos, A., Soldatos, T., Poli, G., Eleftheriadis, G., DelMoro, A., Neiva, A.M., 2007. Interplay between geochemistry and magma dynamics during magma interaction: an example from the Sithonia Plutonic Complex (NE Greece). Lithos 95, 243–266.

Collettini, C., Barchi, M.R., 2002. A low-angle normal fault in the Umbria region (Central Italy): a mechanical model for the related microseismicity. Tectonophysics 359, 97-115.

Collettini, C., Barchi, M R., 2004. A comparison of structural data and seismic images for low-angle normal faults in the Northern Apennines (Central Italy): constraints on activity, in: Alsop, G.I., Holdsworth, R.E., McCaffrey, K.J.W., M Hands (Eds.), Flow processes in faults and shear zones. Geological Society, London, pp. 95-112.

Collettini, C., Holdsworth, R.E., 2004. Fault zone weakening and character of slip along low-angle normal faults: insights from the Zuccale fault, Elba, Italy. J. Geol. Soc. London 161, 1039-1051.

D'Agostino, N., Chamot-Rooke, N., Funiciello, R., Jolivet, L., Speranza, F., 1998. The role of pre-existing thrust faults and topography on the styles of extension in the Gran Sasso range (Central Italy). Tectonophysics 292, 229-254.

Daniel, J.M., Jolivet, L., 1995. Detachment faults and pluton emplacement; Elba Island (Tyrrhenian Sea). Bull. Soc. géol. France 166, 341-354.

de Saint Blanquat, M., Horsman, M.E., Habert, G., Morgan, S., Vanderhaeghe, O., Law, R., Tikoff, B., 2011. Multiscale magmatic cyclicity, duration of pluton construction, and the

paradoxical relationship between tectonism and plutonism in continental arcs. Tectonophysics 500, 20–33, doi:10.10 16/j.tecto.2009.2012.2009.
Denèle, Y., Lecomte, E., Jolivet, L., Lacombe, O., Labrousse, L., Huet, B., Le Pourhiet, L., 2011. Granite intrusion in a metamorphic core complex: the example of the Mykonos laccolith (Cyclades, Greece). Tectonophysics 501, 52-70, doi:10.1016/j.tecto.2011.1001.1013.
Dini, A., Innocenti, F., Rocchi, S., Tonarini, S., Westerman, D.S., 2002. The magmatic evolution of the late Miocene laccolith–pluton–dyke granitic complex of Elba Island, Italy. Geol. Mag. 139, 257–279; DOI: 210.1017/S0016756802006556.
Dini, A., Mazzarini, F., Musumeci, G., Rocchi, S., 2008. Multiple hydro-fracturing by boron-rich fluids in the Late Miocene contact aureole of eastern Elba Island (Tuscany, Italy). Terra Nova 20, 318–326; doi: 310.1111/j.1365-3121.2008.00823.x.
Duchêne, S., Aïssa, R., Vanderhaeghe, O., 2006. Pressure-Temperature-time Evolution of Metamorphic Rocks from Naxos (Cyclades, Greece): constraints from Thermobarometry and Rb/Sr dating Geodynamica Acta 19, 299-319.
Ducoux, M., Branquet, Y., Jolivet, L., Arbaret, L., Grasemann, B., Rabillard, A., Gumiaux, C., Drufin, S., 2016. Synkinematic skarns and fluid drainage along detachments: The West Cycladic Detachment System on Serifos Island (Cyclades, Greece) and its related mineralization. Tectonophysics 695, 1-26; http://dx.doi.org/10.1016/j.tecto.2016.1012.1008.
Duggen, S., Hoernle, K., Van den Bogaard, P., Garbe-Schönberg, D., 2005. Post-Collisional Transition from Subduction- to Intraplate-type Magmatism in the Westernmost Mediterranean: Evidence for Continental-Edge Delamination of Subcontinental Lithosphere.
Duranti, S., Palmeri, R., Pertusati, P.C., Ricci, C.A., 1992. Geological evolution and metamorphic petrology of the sequences of eastern Elba (Complex II). Acta Vulcanologica Marinelli Volume, 213-229.
Faccenna, C., Becker, T.W., 2010. Shaping mobile belts by small-scale convection. Nature 465, 602-605, doi:610.1038/nature09064.
Faccenna, C., Becker, T.W., Auer, L., Billi, A., Boschi, L., Brun, J.P., Capitanio, F.A., Funiciello, F., Horvàth, F., Jolivet, L., Piromallo, C., Royden, L., Rossetti, F., Serpelloni, E., 2014. Mantle dynamics in the Mediterranean. Reviews of Geophysics 52, 283-332; doi:210.1002/2013RG000444.

Faccenna, C., Becker, T.W., Lucente, F.P., Jolivet, L., Rossetti, F., 2001a. History of subduction and back-arc extension in the Central Mediterranean. Geophys. J. Int. 145, 809-820.

Faccenna, C., Funiciello, F., Giardini, D., Lucente, P., 2001b. Episodic back-arc extension during restricted mantle convection in the Central Mediterranean. Earth Planet. Sci. Lett. 187, 105-116.

Farina, F., Dini, A., Innocenti, F., Rocchi, S., Westerman, D.S., 2010. Rapid incremental assembly of the Monte Capanne pluton (Elba Island, Tuscany) by downward stacking of magma sheets. GSA Bulletin 122, 1463–1479; doi: 1410.1130/B30112.30111.

Faulds, J.E., Bouchot, V., Moeck, I., Oguz, K., 2009. Structural control on geothermal systems in Western Turkey: a preliminary report. GRC Transactions 33, 375-381.

Faure, M., Bonneau, M., 1988. Données nouvelles sur l'extension néogène de l'Egée: la déformation ductile du granite miocène de Mykonos (Cyclades, Grèce). *C. R. Acad. Sci. Paris* **307**, 1553-1559.

Faure, M., Bonneau, M., Pons, J., 1991. Ductile deformation and syntectonic granite emplacement during the late Miocene extension of the Aegean (Greece). Bull. Soc. géol. France 162, 3-12.

Fernandez, A., Barbarin, B., 1991. Relative rheology of coeval mafic and felsic magmas: nature of resulting interaction processes and shape and mineral fabric of mafic microgranular enclaves, in: Didier, J., Barbarin, B. (Eds.), Enclaves and Granite Petrology.Development in Petrology, 13 Elsevier, pp. 263–275.

Fernández, C., Castro, A., 2018. Mechanical and structural consequences of magma differentiation at ascent conduits: A possible origin for some mafic microgranular enclaves in granites. Lithos 320–321, 49–61; https://doi.org/10.1016/j.lithos.2018.1009.1004.

Fernandez, A., Gasquet, D., 1994. Relative rheological evolution of chemically contrasted coeval magmas: example of the Tichka plutonic complex (Morocco). Contribution to Mineralogy and Petrology 116, 316–326.

Fernandez, A., Laporte, D., 1984. Signification of low symmetry in magmatic rocks. Journal of structural Geology 13, 337-347.

Ferrara, G., Tonarini, S., 1985. Radiometric geochronology in Tuscany : results and problems. Rend. Soc. Ital. Min. Petrol. 40, 111-124.

Finetti, I.R., Boccaletti, M., Bonini, M., Del Ben, A., Geletti, R., Pipan, M., Sani, F., 2001. Crustal section based on CROP seismic data across the North Tyrrhenian–Northern Apennines–Adriatic Sea. Tectonophysics 343, 135–163.

Gagnevin, D., Daly, J.S., Poli, G., 2004. Petrographic, geochemical and isotopic constraints on magma dynamics and mixing in the Miocene Monte Capanne monzogranite (Elba Island, Italy). Lithos 78, 157–195; doi:110.1016/j.lithos.2004.1004.1043.

Gagnevin, D., Daly, J.S., Poli, G., 2008. Insights into granite petrogenesis from quantitative assessment of the field distribution of enclaves, xenoliths and K-feldspar megacrysts in the Monte Capanne pluton, Italy. Mineralogical Magazine 72, 925–940; DOI: 910.1180/minmag.2008.1072.1184.1925.

Gagnevin, D., Daly, J.S., Horstwood, M.S.A., Whitehouse, M.J., 2011. In-situ zircon U–Pb, oxygen and hafnium isotopic evidence for magma mixing and mantle metasomatism in the Tuscan Magmatic Province, Italy. Earth and Planetary Science Letters 305, 45–56; doi:10.1016/j.epsl.2011.1002.1039.

Gautier, P., Brun, J.P., 1994a. Crustal-scale geometry and kinematics of late-orogenic extension in the central Aegean (Cyclades and Evvia island). Tectonophysics 238, 399-424; doi:310.1016/0040-1951(1094)90066-90063.

Gautier, P., Brun, J.P., 1994b. Ductile crust exhumation and extensional detachments in the central Aegean (Cyclades and Evvia islands). Geodinamica Acta 7, 57-85.

Gautier, P., Brun, J.P., Jolivet, L., 1993. Structure and kinematics of upper Cenozoic extensional detachement on Naxos and Paros (Cyclades Islands, Greece). Tectonics 12, 1180-1194; doi:1110.1029/1193TC01131.

Gerya, T., Yuen, D., 2003. Rayleigh-Taylor instabilities from hydration and melting propel ‘cold plumes’ at subduction zones. Earth Planet. Sci. Lett. 212, 47-62.

Gola, G., Bertini, G., Bonini, M., Botteghi, S., Brogi, A., De Franco, R., Dini, A., Donato, A., Gianelli, G., LiottIa, D., Manzella, A., Montanari, D., Montegrossi, G., Petracchini, L., Ruggieri, G., Santilano, A., Scrocca, D., Trumpy, E., 2017. Data integration and conceptual modelling of the Larderello geothermal area, Italy. Energy Procedia 125, 300-309; 310.1016/j.egypro.2017.1008.1201.

Grasemann, B., Petrakakis, K., 2007. Evolution of the Serifos Metamorphic Core Complex. Journal of the Virtual Explorer 27, 1-18.

Hansen, F.D., Carter, N.L., 1982. Creep of selected crustal rocks at 1000 MPa. Trans. Am. Geophys. Union 63, 437.

Hirschmann, M.M., 2000. Mantle solidus: experimental constraints and the effects of peridotite composition. Geochem. Geophys. Geosyst 1, 2000GC000070.

Huet, B., Labrousse, L., Jolivet, L., 2009. Thrust or detachment? Exhumation processes in the Aegean: insight from a field study on Ios (Cyclades, Greece). Tectonics 28, TC3007, doi:3010.1029/2008TC002397.

Huet, B., Le Pourhiet, L., Labrousse, L., Burov, E., Jolivet, L., 2011. Post-orogenic extension and metamorphic core complexes in a heterogeneous crust: the role of crustal layering inherited from collision. Application to the Cyclades (Aegean domain). Geophysical J. Int. 184, 611–625, doi: 610.1111/j.1365-1246X.2010.04849.x.

Huet, B., Le Pourhiet, L., Labrousse, L., Burov, E., Jolivet, L., 2011. Formation of metamorphic core complex in inherited wedges: a thermomechanical modelling study. Earth Planet. Sci. lett. doi:10.1016/j.epsl.2011.07.004.

Innocenti, F., Westerman, D.S., Rocchi, S., Tonarini, S., 1997. The Montecristo monzogranite (Northern Tyrrhenian Sea, Italy): a collisional pluton in an extensional setting. Geological Journal 32, 131-151.

Jansen, J.B.H., 1977. Metamorphism on Naxos, Greece. Utrecht University.

Jolivet, L., Augier, R., Faccenna, C., Negro, F., Rimmele, G., Agard, P., Robin, C., Rossetti, F., Crespo-Blanc, A., 2008. Subduction, convergence and the mode of backarc extension in the Mediterranean region. Bull Soc géol France 179, 525-550.

Jolivet, L., Brun, J.P., 2010. Cenozoic geodynamic evolution of the Aegean region. Int. J. Earth Science 99, 109–138, DOI: 110.1007/s00531-00008-00366-00534.

Jolivet, L., Daniel, J.M., Truffert, C., Goffé, B., 1994. Exhumation of deep crustal metamorphic rocks and crustal extension in back-arc regions. Lithos 33, 3-30; doi:10.1016/0024-4937(1094)90051-90055.

Jolivet, L., Faccenna, C., 2000. Mediterranean extension and the Africa-Eurasia collision. Tectonics 19, 1095-1106; doi:1010.1029/2000TC900018.

Jolivet, L., Faccenna, C., Goffé, B., Mattei, M., Rossetti, F., Brunet, C., Storti, F., Funiciello, R., Cadet, J.P., Parra, T., 1998. Mid-crustal shear zones in post-orogenic extension: the northern Tyrrhenian Sea case. J. Geophys. Res. 103, 12123-12160; doi:12110.11029/12197JB03616.

Jolivet, L., Lecomte, E., Huet, B., Denèle, Y., Lacombe, O., Labrousse, L., Le Pourhiet, L., Mehl, C., 2010. The North Cycladic Detachment System. Earth and Planet. Sci. Lett. 289 87-104, doi:110.1016/j.epsl.2009.1010.1032.

Jolivet, L., Menant, A., Sternai, P., Rabillard, A., Arbaret, L., Augier, R., Laurent, V., Beaudoin, A., Grasemann, B., Huet, B., Labrousse, L., Le Pourhiet, L., 2015. The geological signature of a slab tear below the Aegean. Tectonophysics 659 166–182, 166–182, doi:110.1016/j.tecto.2015.1008.1004.

Jolivet, L., Sautter, V., Moretti, I., Vettor, T., Papadopoulou, Z., Augier, R., Denèle, Y., Arbaret, L., 2021. Anatomy and evolution of a migmatite-cored extensional metamorphic dome and interaction with syn-kinematic intrusions, the Mykonos-Delos-Rheneia MCC. Journal of Geodynamics, accepted.

Juteau, M., Michard, A., Zimmermann, J.L., Albarede, F., 1984. Isotopic heterogeneities in the granitic intrusion of Monte Capanne (Elba island, Italy) and dating concepts. Journal of Petrology 25, 532-545.

Katzir, Y., Matthews, A., Garfunkel, Z., Schliestedt, M., Avigad, D., 1996. The tectono-metamorphic evolution of a dismembered ophiolite (Tinos, Cyclades, Greece). Geol. Mag. 133, 237-254.

Keay, S., Lister, G., Buick, I., 2001. The timing of partial melting, Barrovian metamorphism and granite intrusion in the Naxos metamorphic core complex, Cyclades, Aegean Sea, Greece. Tectonophysics 342, 275-312; doi:210. 1016/S0040-1951(1001)00168-00168.

Keller, J.V., Pialli, G., 1990. Tectonics of the island of Elba: a reappraisal. Boll. Soc. Geol. It. 109, 413-425.

Keller, J.V.A., Minelli, G., Pialli, G., 1994. Anatomy of late orogenic extension: the Northern Apennines case. Tectonophysics 238, 275-294.

Kruckenberg, S.C., Vanderhaeghe, O., Ferré, E.C., Teyssier, C., Whitney, D.L., 2011. Flow of partially molten crust and the internal dynamics of a migmatite dome, Naxos, Greece: internal dynamics of the Naxos dome. Tectonics 30, 1–24, doi:10.1029/2010TC002751.

Kuhlemann, J., Frisch, W., Dunkl, I., Kázmér, M., Schmiedl, G., 2004. Miocene siliciclastic deposits of Naxos Island: Geodynamic and environmental implications for the evolution of the southern Aegean Sea (Greece), in: Bernet, M., Spiegel, C. (Eds.), Detrital thermochronology - Provenance analysis, exhumation, and landscape evolution of mountain belts:. Geological Society of America, pp. 51-65.

Labrousse, L., Huet, B., Le Pourhiet, L., Jolivet, L., Burov, E., 2016. Rheological implications of extensional detachments: Mediterranean and numerical insights. Earth-Science Reviews 161, 233-258; http://dx.doi.org/210.1016/j.earscirev.2016.1009.1003.

Lamont, T.N., Roberts, N.M.W., Searle, M.P., Gopon, P., Waters, D.J., Millar, I., 2020. The age, origin, and emplacement of the Tsiknias Ophiolite, Tinos, Greece. Tectonics 39, e2019TC00567; https://doi.org/ 00510.01029/02019TC005677.

Laurent, V., Beaudoin, A., Jolivet, L., Arbaret, L., Augier, R., Rabillard, A., 2015. Interrelations between extensional shear zones and synkinematic intrusions: The example of Ikaria Island (NE Cyclades, Greece). Tectonophysics 651-652, 152-171, http://dx.doi.org/110.1016/j.tecto.2015.1003.1020.

Lee, J., Lister, G.S., 1992. Late Miocene ductile extension and detachment faulting, Mykonos, Greece. Geology 20, 121-124; doi:110.1130/0091-7613(1992)1020<0121:LMDEAD>1132.1133.CO;1132.

Le Pourhiet, L., Burov, E., Moretti, I., 2004. Rifting through a stack of inhomogeneous thrusts (the dipping pie concept). Tectonics 23, doi:10.1029/2003TC001584.

Lecomte, E., Le Pourhiet, L., Lacombe, O., 2012. Mechanical basis for the activity of low angle normal faults. Geophysical Res. Lett. 39, L03307; doi:03310.01029/02011GL050756.

Lecomte, E., Le Pourhiet, L., Lacombe, O., Jolivet, L., 2011. A continuum mechanics approach to quantify brittle strain on weak faults: application to the extensional reactivation of shallow-dipping discontinuities. Geophys. J. Int. 184, 1-11, doi: 10.1111/j.1365-1246X.2010.04821.x.

Liotta, D., Brogi, A., Árnadóttir, S., Ágústsson, K., Thorsteinsdóttir, U., 2021. Field evidence of the interplay between rift and transform structures in the Krafla geothermal area, N-Iceland. Geothermics 91, 102039; https://doi.org/102010.101016/j.geothermics.102020.102039.

Liotta, D., Brogi, A., Meccheri, M., Dini, A., Bianco, C., Ruggieri, G., 2015. Coexistence of low-angle normal and high-angle strike- to oblique-slip faults during Late Miocene mineralization in eastern Elba Island (Italy). Tectonophysics 660, , 17-34; http://dx.doi.org/10.1016/j.tecto.2015.1006.1025.

Lister, G.S., Baldwin, S., 1993. Plutonism and the origin of metamorphic core complexes. Geology 21, 607-610; doi:610.1130/0091-7613(1993)1021<0607:PATOOM>1132.1133.CO;1132.

Lister, G.S., Snoke, A.W., 1984. S-C mylonites. Journal of Structural Geology 6, 617-638.

Maineri, C., Benvenuti, M., Costagliola, P., Dini, A., Lattanzi, P., Ruggieri, G., Villa, I.M., 2003. Sericitic alteration at the La Crocetta deposit (Elba Island, Italy): interplay between magmatism, tectonics and hydrothermal activity. Mineralium Deposita 38, 67–86; DOI 10.1007/s00126-00002-00279-00122.

Mantovani, E., Viti, M., Babbucci, D., Tamburelli, C., Cenni, N., 2020. Geodynamics of the central-western Mediterranean region: plausible and non-plausible driving forces. Marine and Petroleum Geology 113, 104121.

Martha, S.O., Dörr, W., Gerdes, A., Petschick, R., Schastok, J., Xypolias, P., Zulauf, G., 2016. New structural and U–Pb zircon data from Anafi crystalline basement (Cyclades, Greece): constraints on the evolution of a Late Cretaceous magmatic arc in the Internal Hellenides. International Journal of Earth Sciences 105, 2031–2060, doi:2010.1007/s00531-00016-01346-00538.

Massa, G., Musumeci, G., Mazzrini, F., Pieruccioni, D., 2017. Coexistence of contractional and extensional tectonics during the northern Apennines orogeny: the late Miocene out-of-sequence thrust in the Elba Island nappe stack. Geological Journal 52, 353–368; DOI: 310.1002/gj.2761.

Mazzarini, F., Musumeci, G., Cruden, A.R., 2011. Vein development during folding in the upper brittle crust: The case of tourmaline-rich veins of eastern Elba Island, northern Tyrrhenian Sea, Italy. Journal of Structural Geology 33, 1509-1522; doi:1510.1016/j.jsg.2011.1507.1001.

Menant, A., Jolivet, L., Augier, R., Skarpelis, N., 2013. The North Cycladic Detachment System and associated mineralization, Mykonos, Greece: insights on the evolution of the Aegean domain. Tectonics 32, 433–452, doi:410.1002/tect.20037.

Menant, A., Jolivet, L., Vrielynck, B., 2016. Kinematic reconstructions and magmatic evolution illuminating crustal and mantle dynamics of the eastern Mediterranean region since the late Cretaceous. Tectonophysics 675, 103-140; doi: 110.1016/j.tecto.2016.1003.1007.

Mezri, L., Le Pourhiet, L., Wolf, S., Burov, E., 2015. New parametric implementation of metamorphic reactions limited by water content, impact on exhumation along detachment faults. Lithos 236-237, 287-298; http://dx.doi.org/210.1016/j.lithos.2015.1008.1021..

Miller, C.F., McDowell, S.M., Mapes, R.W., 2003. Hot and cold granites? Implications of zircon saturation temperatures and preservation of inheritance. Geology 31, 529-532.

Moeller, S., Grevemeyer, I., Ranero, C., Berndt, C., Klaeschen, D., Sallares, V., Zitellini, N., de Franco, R., 2013. Early-stage rifting of the northern Tyrrhenian Sea Basin: Results from a combined wide-angle and multichannel seismic study. Geochem. Geophys. Geosyst. 14, , 3032–3052, doi:3010.1002/ggge.20180.

Moeller, S.I., Grevemeyer, C.R., Ranero, C.R., Berndt, C., Klaeschen, D., Sallares, V., Zitellini, N., de Franco, R., 2014. Crustal thinning in the northern Tyrrhenian Rift: Insights from multi- channel and wide-angle seismic data across the basin. J. Geophys. Res. Solid Earth 119, 1655–1677, doi:1610.1002/ 2013JB010431.

Musumeci, G., Mazzarini, F., Cruden, A.R., 2015. The Zuccale Fault,Elba Island, Italy: A new perspective from fault architecture. Tectonics 34, 1195–1218, doi:1110.1002/2014TC003809.

Musumeci, G., Vaselli, L., 2012. Neogene deformation and granite emplacement in the metamorphic units of northern Apennines (Italy): Insights from mylonitic marbles in the Porto Azzurro pluton contact aureole (Elba Island). Geosphere 8, 470–490; doi:410.1130/GES00665.00661.

Pandeli, E., Giusti, R., Elter, F.M., Orlando, A., Orti, L., 2018. Structural setting and metamorphic evolution of a contact aureole: the example of the Mt. Capanne pluton (Elba Island, Tuscany, italy). Ofioliti 43, 41-73; doi: 10.4454/ofioliti.v4443i4451.4455.

Papeschi, S., Musumeci, G., Massonne, H.J., Bartoli, O., Cesare, B., 2019. Partial melting and strain localization in metapelites at very low-pressure conditions: The northern Apennines magmatic arc on the Island of Elba, Italy. Lithos 350-351, 105230; https://doi.org/105210.101016/j.lithos.102019.105230.

Papeschi, S., Musumeci, G., Mazzarini, F., 2017. Heterogeneous brittle-ductile deformation at shallow crustal levels under high thermal conditions: The case of a synkinematic contact aureole in the inner northern Apennines, southeastern Elba Island, Italy. Tectonophysics 717, 547–564.

Papeschi, S., Musumeci, G., Mazzarini, F., 2018. Evolution of shear zones through the brittle-ductile transition: The Calamita Schists (Elba Island, Italy). Journal of Structural Geology 113, 100–114.

Paterson, S.R., 2009. Magmatic tubes, pipes, troughs, diapirs, and plumes: Late-stage convective instabilities resulting in compositional diversity and permeable networks in crystal-rich magmas of the Tuolumne batholith, Sierra Nevada, California. Geosphere 5, 496–527; doi: 410.1130/GES00214.00211.

Pauselli, C., Ranalli, G., 2017. Effects of lateral variations of crustal rheology on the occurrence of post- orogenic normal faults: The Alto Tiberina Fault (Northern Apennines, Central Italy). Tectonophysics 721, 45-55; http://dx.doi.org/10.1016/j.tecto.2017.1009.1008.

Pe-Piper, G., 2000. Origin of S-type granites coeval with I-type granites in the Hellenic subduction system, Miocene of Naxos, Greece. European Journal of Mineralogy 12, 859–875, doi:810.1127/ejm/1112/1124/0859.

Pe-Piper, G., Kotopouli, C.N., Piper, D.J.W., 1997. Granitoid rocks of Naxos, Greece: regional geology and petrology. Geological Journal 32, 153–171, doi:110.1002/(SICI)1099-

1034(199706)199732: 199702<199153::AID-GJ199737>199703.199700.CO;199702-199701.

Pe-Piper, G., Piper, D.J.W., 2002. The igneous rocks of Greece. The anatomy of an orogen. Gebrüder Borntraeger, Berlin-Stuttgart.

Pe-Piper, G., Piper, D.J.W., 2007. Neogene back-arc volcanism of the Aegean: new insights into the relationship between magmatism and tectonics, in: Beccaluva, L., Bianchini, G. (Eds.), Cenozoic Volcanism in the Mediterranean Area. Geological Society of America, pp. 17–31, doi: 10.1130/2007.2418(1102).

Pe-Piper, G., Piper, D.J.W., Matarangas, D., 2002. Regional implications of geochemistry and style of emplacement of Miocene I-type diorite and granite, Delos, Cyclades, Greece. Lithos 60, 47–66, doi:10.1016/S0024-4937(1001)00068-00068.

Perrin, M., 1975. L'ile d'Elbe et la limite Alpes-Apennins: données sur la structure géologique et l'évolution tectogénétique de l'Elbe alpine et de l'Elbe apennine. Bull. Soc. Geol. It. 94, 1929-1955.

Pertusati, P.C., Raggi, G., Ricci, C.A., Duranti, S., Palmeri, R., 1993. Evoluzione post-collisionale dell'Elba centro-orientale. Mem. Soc. Geol. It. 49, 297-312.

Perugini, D., Poli, G., Rocchi, S., 2005. Development of viscous fingering between mafic and felsic magmas: evidence from the Terra Nova Intrusive Complex (Antarctica). Mineralogy and Petrology 83, 151–166.

Petrakakis, K., Iglseder, C., Zámolyi, A., Rambousek, C., Grasemann, B., Draganitis, E., Kurka, A., Photiades, A., 2010. Serifos Island, Geological Map of Greece. Institute of Geology and Mineral Exploration (IGME).

Poli, G., Manetti, P., Tommasini, S., 1989. A petrological review on Miocene–Pliocene intrusive rocks from Southern Tuscany and Tyrrhenian Sea (Italy). Periodico di Mineralogia 58, 109 – 126.

Poli, G.E., Tommasini, S., 1991. Model for the Origin and Significance of Microgranular Enclaves in Calc-alkaline Granitoids. Journal of Petrology 32, 657-666.

Rabillard, A., Arbaret, L., Jolivet, L., Le Breton, N., Gumiaux, C., Augier, R., Grasemann, B., 2015. Interactions between plutonism and detachments during Metamorphic Core Complex formation, Serifos Island (Cyclades, Greece). Tectonics 34, 1080-1106, DOI: 1010.1002/2014TC003650.

Rabillard, A., Jolivet, L., Arbaret, L., Bessière, E., Laurent, V., Menant, A., Augier, R., Beaudoin, A., 2018. Synextensional Granitoids and Detachment Systems Within

Cycladic Metamorphic Core Complexes (Aegean Sea, Greece): Toward a Regional Tectonomagmatic Model. Tectonics 37; https://doi.org/10.1029/2017TC004697.

Ranalli, G., Murphy, D.C., 1987. Rheological stratification of the lithosphere. Tectonophysics 132, 281-295.

Reinecke, T., Altherr, R., Hartung, B., Hatzipanagiotou, K., Kreuzer, H., Harre, W., Klein, H., Keller, J., Geenen, E., Böger, H., 1982. Remnants of a late Cretaceous high temperature bet on the island of Anafi (Cyclades, Greece). N. Jb. Miner. Abh 145, 157-182.

Rey, P.F., Teyssier, C., Whitney, D.L., 2009. The Role of Partial Melting and Extensional Strain Rates in the Development of Metamorphic Core Complexes. Tectonophysics 477, 135-144, doi: 110.1016/j.tecto.2009.1003.1010.

Ring, U., 2007. The geology of Ikaria Island: The Messaria extensional shear zone, granites and the exotic Ikaria nappe. Journal of the Virtual Explorer 27, 1–32.

Ring, U., Glodny, J., Will, T., Thomson, S., 2010. The Hellenic Subduction System: High-Pressure Metamorphism, Exhumation, Normal Faulting, and Large-Scale Extension. Annu. Rev. Earth Planet. Sci. 38, 45–76, 10.1146/annurev.earth.050708.170910.

Rocchi, S., Westerman, D.S., Dini, A., Innocenti, F., Tonarini, S., 2002. Two-stage growth of laccoliths at Elba Island, Italy. Geology 30, 983–986.

Roche, V., Bouchot, V., Beccaletto, L., Jolivet, L., Guillou-Frottier, L., Tuduri, J., Bozkurt, E., Oguz, K., Tokay, B., 2018a. Structural, lithological and geodynamic controls on geothermal activity in the Menderes geothermal Province (Western Anatolia, Turkey). Int J Earth Sci (Geol Rundsch) in press, https://doi.org/10.1007/s00531-00018-01655-00531.

Roche, V., Sternai, P., Guillou-Frottier, L., Menant, A., Jolivet, L., Bouchot, V., Gerya, T., 2018. Emplacement of metamorphic core complexes and associated geothermal systems controlled by slab dynamics. Earth and Planetary Science Letters 498 322–333; https://doi.org/310.1016/j.epsl.2018.1006.1043.

Rochira, F., Caggianelli, A., de Lorenzo, S., 2018. Regional thermo-rheological field related to granite emplacement in the upper crust: implications for the Larderello area (Tuscany, Italy). Geodinamica Acta 30, 225-240, DOI: 210.1080/09853111.09852018.01488912.

Rodríguez, C., Castro, A., 2019. Origins of mafic microgranular enclaves and enclave swarms in granites: Field and geochemical relations. GSA Bulletin 131, 635–660; https://doi.org/610.1130/B32028.32021.

Romagny, A., Jolivet, L., Menant, A., Bessière, E., Maillard, A., Canva, A., Thinon, I., 2020. Detailed tectonic reconstructions of the Western Mediterranean region for the last 35 Ma, insights on driving mechanisms. BSGF-Earth Sciences Bulletin 191, 37, https://doi.org/10.1051/bsgf/2020040.

Rosenberg, C.L., Handy, M.R., 2005. Experimental deformation of partially melted granite revisited: implications for the continental crust. Journal of metamorphic Geology 23

Rossetti, F., Balsamo, F., Villa, I.M., Bouybaouenne, M., Faccenna, C., Funiciello, R., 2008. Pliocene-Pleistocene HT-LP metamorphism during multiple granitic intrusions in the southern branch of the Larderello geothermal field (southern Tuscany, Italy). J. Geol. Soc. London 165, 247-262.

Rossetti, F., Faccenna, C., Jolivet, L., Funiciello, R., Goffé, B., Tecce, F., Brunet, C., Monié, P., Vidal, O., 1999. Structural signature and exhumation P-T-t path of the Gorgona blueschist sequence (Tuscan Archipelago, Italy). Ofioliti 26, 175-186.

Rossetti, F., Tecce, F., 2008. Composition and evolution of fluids during skarn development in the Monte Capanne thermal aureole, Elba Island, central Italy. Geofluids 8 167–180; doi: 110.1111/j.1468-8123.2008.00215.x.

Rossetti, F., Tecce, F., Billi, A., Brilli, M., 2007. Patterns of fluid flow in the contact aureole of the Late Miocene Monte Capanne pluton (Elba Island, Italy): the role of structures and rheology. Contrib Mineral Petrol 53, 743–760; DOI 710.1007/s00410-00006-00175-00413.

Ryan, E., Papeschi, S., Viola, G., Musumeci, G., Mazzarini, F., Torgersen, E., Sørensen, B.E., Ganerød, M., 2021. Syn-orogenic exhumation of high-P units by upward extrusion in an accretionary wedge: insights from the Eatsren Elba nappe stack (Northern Apennines, Italy).

Salemink, J., 1985. Skarn and ore formation at Serifos, Greece, as a consequence of granodiorite intrusion. University of Utrecht, Netherlands.

Sanchez-Gomez, M., Avigad, D., Heiman, A., 2002. Geochronology of clasts in allochthonous Miocene sedimentary sequences on Mykonos and Paros islands: implications for back-arc extension in the Aegean Sea. J. Geol. Soc. London 159, 45-60; doi:10.1144/0016-764901031.

Saupé, F., Marignac, C., Moine, B., Sonet, J., Zimmermann, J.L., 1982. Datation par les méthodes K/Ar et Rb/Sr de quelques roches de la partie orientale de l'ile d'Elbe (Province de Livourne, Italie). Bulletin de Minéralogie 105, 236-245.

Savelli, C., 1988. Late Oligocene to Recent episodes of magmatism in and around the Tyrrhenian Sea: implication for the process of opening in a young inter-arc basin of intra-orogenic (Mediterranean) type. Tectonophysics 146, 163-181.

Savelli, C., 2002a. Tectono-magmatic lineaments and subduction in the central Mediterranean and southern Italy during the past 8 Ma. Boll. Soc. Geol. It., 121, 231-242.

Savelli, C., 2002b. Time–space distribution of magmatic activity in the western Mediterranean and peripheral orogens during the past 30 Ma (a stimulus to geodynamic considerations). Journal of Geodynamics 34, 99–126.

Savelli, C., 2015. Fast Episodes of West- Mediterranean-Tyrrhenian Oceanic Opening and Revisited Relations with Tectonic Setting. Scientific Reports 5:, 14271; DOi: 14210.11038/srep14271.

Scheffer, C., Vanderhaeghe, O., Lanari, P., Tarantola, A., Ponthus, L., Photiades, A., France, L., 2016. Syn- to post-orogenic exhumation of metamorphic nappes: Structure and thermobarometry of the western Attic-Cycladic metamorphic complex (Lavrion, Greece). Journal of Geodynamics 96, 174–193; http://dx.doi.org/110.1016/j.jog.2015.1008.1005.

Schubert, M., Driesner, T., Gerya, T.V., Ulmer, P., 2013. Mafic injection as a trigger for felsic magmatism: A numerical study. Geochem. Geophys. Geosyst. 14, 1910–1928, doi:1910.1002/ggge.20124.

Serri, G., Innocenti, F., Manetti, P., 1993. Geochemical and petrological evidence of the subduction of delaminated Adriatic continental lithosphere in the genesis of the Neogene-Quaternary magmatism of central Italy. Tectonophysics 223, 117-147.

Seward, D., Vanderhaeghe, O., Siebenaller, L., Thomson, S., Hibsch, C., Zingg, A., Holzner, P., Ring, U., Duchêne, S., 2009. Cenozoic tectonic evolution of Naxos Island through a multi-faceted approach of fission-track analysis, in: Ring, U., Wernicke, B. (Eds.), Extending a continent: architecture, rheology and heat budget. Geological Society, London, pp. 179-196; doi:110.1144/SP1321.1149.

Soukis, K.I., Papanikolaou, D.J., 2004. Contrasting geometry between Alpine and Late-to-post-Alpine tectonic structures in Anafi Island (Cyclades). Bulletin of the Geological Society of Greece vol. 2004 XXXVI, 1688-1696.

Spakman, W., Wortel, R., 2004. A tomographic view on Western Mediterranean geodynamics, in: Cavazza, W., Roure, F.M., Spakman, W., Stampfli, G.M., Ziegler, P.A. (Eds.), The TRANSMED Atlas - The Mediterranean region from crust to Mantle. Springer, Berlin, Heidelberg, pp. 31-52.

Spiess, R., Langone, A., Caggianelli, A., Stuart, F.M., Zucchi, M., Bianco, C., Brogi, A., Liotta, D., 2021. Unveiling ductile deformation during fast exhumation of a granitic pluton in a transfer zone. Journal of Structural Geology, https://doi.org/10.1016/j.jsg.2021.104326.

St. Seymour, K., Zouzias, D., Tombros, S., Kolaiti, E., 2009. Geochemistry of the Serifos pluton (Cycladic islands) and associated iron oxide and sulfide ores: Skarn or metamorphosed exhalite deposits? Neues Jahrbuch für Mineralogie - Abhandlungen 186, 249-270; doi:210.1127/0077-7757/2009/0143.

Thompson, A.B., Connolly, J.A.D., 1995. Melting of the continental crust: some thermal and petrological constraints on anatexis in continental collision zones and other tectonic settings. J. Geoph. Res. 100, 15565-15579.

Tirel, C., Brun, J.P., Burov, E., 2004. Thermo-mechanical modeling of extensional gneiss domes, in: Whitney, D.L., Teyssier, C., Siddoway, C.S. (Eds.), Gneiss domes in orogeny, Boulder, Colorado, pp. 67-78.

Tirel, C., Brun, J.P., Burov, E., 2008. Dynamics and structural development of metamorphic core complexes. J. Geoph. Res. 113, doi:10.1029/2005JB003694.

Tombros, S.F., St. Seymour, K., Williams-Jones, A.E., Zhai, D., Liu, J., 2015. Origin of a barite-sulfide ore deposit in the Mykonos intrusion, cyclades: Trace element, isotopic, fluid inclusion and raman spectroscopy evidence. Ore Geology Reviews 67, 139–157; http://dx.doi.org/110.1016/j.oregeorev.2014.1011.1016.

Trevisan, L., 1950. L'Elba orientale e la sua tettonica scivolamento par gravità. Mem. Instit. Geol. It. Pavia 70, 435-470.

Urai, J.L., Shuiling, R.D., Jansen, J.B.H., 1990. Alpine deformation on Naxos (Greece), in: Knipe, R.J., Rutter, E.H. (Eds.), Deformation mechanisms, Rheology and tectonics. *Geol. Soc. spec. Pub.*, pp. 509-522; doi:510.1144/GSL.SP.1990.1054.1101.1147.

van der Laan, S.R., Wyllie, P.J., 1993. Experimental Interaction of Granitic and Basaltic Magmas and Implications for Mafic Enclaves. Journal of Petrology 34, 491-517.

Vanderhaeghe, O., 2004. Structural development of the Naxos migmatite dome, in: Whitney, D.L., Teyssier, C., Siddoway, C.S. (Eds.), Gneiss domes in orogeny. Geological Society of America, Boulder, Colorado, pp. 211-227.

Vanderhaeghe, O., Kruckenberg, S.C., Gerbault, M., Martin, L., Duchêne, S., Deloule, S., 2018. Crustal-scale convection and diapiric upwelling of a partially molten T orogenic root (Naxos dome, Greece). Tectonophysics 746; https://doi.org/10.1016/j.tecto.2018.03.007, 459–469

Vernon, R.H., 1986. K-feldspar megacrysts in granites - phenocrysts, not porphyroblasts. Earth-Sci. Rev. 23, 1-63.

Vernon, R.H., Paterson, S.R., 2008. How late are K-feldspar megacrysts in granites? Lithos 104, 327–336; doi:310.1016/j.lithos.2008.1001.1001.

Viola, G., Torgersen, E., Mazzarini, F., Musumeci, G., van der Lelij, R., Schönenberger, J., Garofalo, P.S., 2018. New constraints on the evolution of the inner Northern Apennines by K-Ar dating of Late Miocene-Early Pliocene compression on the Island of Elba, Italy. Tectonics 37, 3229–3243. https://doi.org/3210.1029/ 2018TC005182.

Weinberg, R.F., Hasalová, P., 2015. Water-fluxed melting of the continental crust: A review. Lithos 212–215, 158–188; http://dx.doi.org/110.1016/j.lithos.2014.1008.1021.

Weinberg, R.F., Sial, A.N., Pessoa, R.R., 2001. Magma flow within the Tavares pluton, Northeastern Brazil: compositional and thermal convection. Bull. Geol. Soc. Am. 113, 508–520.

Westerman, D.S., Dini, A., Innocenti, F., Rocchi, S., 2004. Rise and fall of a nested Christmas-tree laccolith complex, Elba Island, Italy, in: Breitkreuz, C., Petford, N. (Eds.), Physical geology of high level magmatic systems. Geological Society, London, pp. 195-213.

Westerman, D.S., Innocenti, F., Tonarini, S., Ferrara, G., 1993. The Pliocene intrusions of the island of Giglio. Mem. Soc. Geol. It. 49, 345-363.

Wiebe, R.A., Jellinek, A.M., Hodge, K.F., 2017. New insights into the origin of ladder dikes: Implications for punctuated growth and crystal accumulation in the Cathedral Peak granodiorite. Lithos 277, 241–258; http://dx.doi.org/210.1016/j.lithos.2016.1009.1015.

Wortel, M.J.R., Spakman, W., 2000. Subduction and slab detachment in the Mediterranean-Carpathian region. Science 290, 1910-1917.

Figure captions

Figure 1: Present-day tectonic context of the Mediterranean region and two reconstructions at 5 and 15 Ma showing the position of volcanic edifices and plutons with an emphasis on the cases of the Cyclades and Elba Island addressed in this paper. These reconstructions are taken and modified from Romagny et al. (2020).

Figure 2: Tectonic map of the Aegean region showing the successive generations of granitoids since the late Cretaceous. Modified from Jolivet et al. (2015). Background topography was extracted from GeoMapApp.

Figure 3: Tectonic map of the Central and Western Mediterranean with the distribution of recent magmatism (Savelli, 1988; Serri et al., 1993; Savelli, 2002b, a; Duggen et al., 2005; Avanzinelli et al., 2009; Savelli, 2015). Tectonic map (B) of the northern Tyrrhenian region and Northern Apennines and (C) a diagram showing the evolution of the ages of syn-rift basins, metamorphic events and magmatism along a cross-section from Corsica to the Apennines, modified from Jolivet et al. (1998).

Figure 4: Two lithospheric-scale cross-sections of the Aegean domain (Jolivet and Brun, 2010) and the Northern Tyrrhenian Sea and the Apennines (Jolivet et al., 1998).

Figure 5: Five examples of the Aegean granitoids showing the interactions between deformation and intrusion, after Rabillard et al. (2018) and references therein. Maps of the left column show maps of the entire islands and the right column shows the internal fabrics of the plutons. These maps were obtained based on deformation grades observed in the field, a scale of grades was designed for each pluton to describe the gradients. Arrows show stretching lineations and sense of shear and black bars on the Tinos pluton shows the direction of the magnetic lineation.

Figure 6: Details of the two detachments on Mykonos and Serifos. A: northeastern Mykonos (see location on figure 5), B: Southwest Serifos. The Mykonos (MD) and Livada (LD) detachments on Mykonos and the mineralized veins and normal faults (baryte and iron-hydroxides) – grey- are after Menant et al. (2013). The Kàvos Kiklopas (KKD) and

Meghàlo Livadi (MLD) detachments on Serifos are after Grasemann and Petrakakis (2007) and Ducoux et al. (2016).

Figure 7: Tectonic map and cross-section of Elba Island showing the main tectonic units and the main extensional shear zones and detachments, modified after Bianco et al. (2015). Details of the internal structure of the Monte Capanne intrusions are reported based on Farina et al. (2010).

Figure 8: Photographs of the Sant' Andrea facies in the Monte Capanne pluton and of the deformation along the eastern margin of the pluton, in the pluton itself and in the contact metamorphic aureole. A: general view of the orientation of K-feldspar megacrysts and some mafic enclaves. B: Detailed view of the oriented K-feldspar megacrysts (horizontal plane). C: zoom on the orientation of K-feldspar megacrysts (vertical plane). D: Cotoncello dyke. E: cluster of K-feldspar megacrysts in the vicinity of the Cotoncello dyke. F: Mylonitic foliation within the Monte Capanne shear zone. G: Sigmoidal foliation and top-to-the-east sense of shear within the metamorphic aureole of the Monte Capanne pluton. H: detailed view of syn-kinematic contact metamorphism garnets in veins perpendicular to the regional stretching direction.

Figure 9: Photographs of the Zucalle detachment and its internal structure. Upper: overview of the detachment fault. Lower left: Detail of the contact zone and the truncated foliation in the hanging wall. Lower right: detail of the shear bands indicating top-to-the east kinematics.

Figure 10: Photographs of the root zone of the Sant'Andrea facies in the melange zone in and around the Cotoncello dyke. A: Schlieren with cross-bedding. B: Mush zone with cluster of K-feldspar megacrysts and mafic enclaves. C: Isolated blob of mush zone with large K-feldspar megacrysts. D: Folded alternation of leucocratic and melanocratic layers with schlierens. E: Detail of D, schlieren. F: detail of D: schlieren tube.

Figure 11: Photographs of large mafic enclaves and melange zones in the westernmost part of the Sant'Andrea facies showing the disorientation of K-feldspar megacrysts and melange facies (mingling).

Figure 12: Detailed study of the orientation of K-feldspar megacrysts in the Sant-Andrea facies with foliation trajectories.

Figure 13: Schematic section showing a conceptual model of the relations between syn-kinematic plutons and the detachments, based on the examples of the Aegean and North Tyrrhenian plutons. Modified from Rabillard et al. (2018).

Figure 14: Conceptual model of the succession of events leading to the emplacement of a plutonic system below an active series of detachments, based on Huet et al. (2011) and Schubert et al. (2013).

Figure 15: Snapshots of the numerical experiments with two different liquidus temperatures (950°C and 1000°C) from 2 to 12.5 Myr. White line limits the molten lower crust with melt ration above 40% (pluton).

Figure 16: Zoom of the last 5 Ma of evolution of the model of figure 15 with a liquidus temperature of 1000°C from 15Myr to 19.8 Myr (black dotted rectangle on figure 15 for location).

Figure 17: Structural cross-section based on the most evolved stage of the numerical model at 19.8 Myr.

Appendix A Table A1

		Sediments (2)	Upper crust (1)	Middle crust(2)	Lower crust(1)	Lithospheric mantle(3)	Asthenospheric mantle(3)
Density(kg.m^{-3})	ρ_r	2400	2700	2700	2700	3300	3300
Pre exp. Factor (MPa^{-n}s^{-1})	A	2.4	3.3	2.4	3.3	3.5	3.5
Activation energy(kJ)	Q	156	186	156	219	532	532
Stress exponent	n	$6.7\ 10^{-6}$	$2\ 10^{-6}$	$6.7\ 10^{-6}$	$1.3\ 10^{-3}$	$2.5\ 10^{4}$	$2.5\ 10^{4}$
Melt density(kg.m^{-3})	ρ_m	-	2400	2400	2400	2800	2800
Melt viscosity	η_m	-	10^{17}	10^{17}	10^{17}	10^{12}	10^{12}
Heat production (Wm^{-3})	H	$1.67\ 10^{-10}$	$1.67\ 10^{-10}$	0	0	0	0
Thermal diffusivity	κ	10^{-6}	10^{-6}	10^{-6}	10^{-6}	10^{-6}	$5\ 10^{-6}$

Table A1 : Values and notation for variable physical parameters. Parameters for dislocation creep come from 1 (Ranalli and Murphy, 1987), 2 (Hansen and Carter, 1982) and 3 (Chopra and Paterson, 1984). Other constant parameters include: friction ϕ and cohesion C which varies linearly with plastic strain in range [0,1] respectively from 30° to 20° and from 20 MPas to 2 MPa; Coefficient of thermal expansion and compressibility that are set to $3.10^{-5}K^{-1}$ and 10^{-11} Pa^{-1}.

Appendix A, figure caption:

Figure A1: MgO v. Si02 Harker diagram showing the negative correlation between whole rock MgO and SiO_2 content for three, I-type hornblende-biotite bearing, representative Aegean granites. Data from Delos intrusion (Pe-Piper et al., 2002), Serifos (Salemink, 1985) and Naxos (Pe-Piper et al., 1997). Mixing/mingling processes between mafic mantle-derived melts and acid magmas produce composite batholiths (Poli and Tommasini, 1990) as illustrated by the case of the Elba Island magmatic complex showed for comparison (See Dini et al. 2002 for explanation). MME = Mafic Microgranular Enclaves.

Figure A2: Solidus and liquidus as a function of pressure and temperature for mantle and crust (950 and 1000°C).

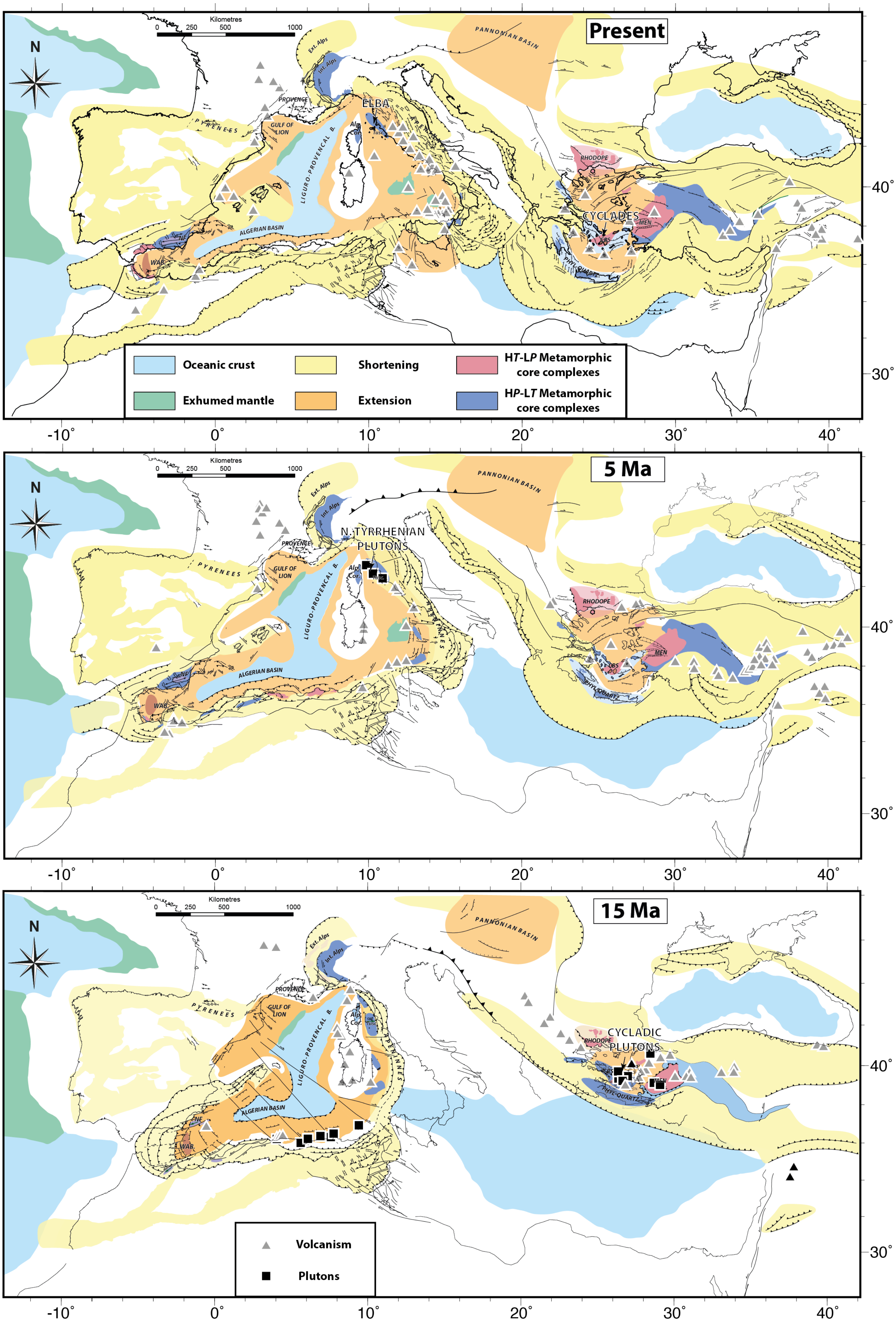

Figure 1: Present-day tectonic context of the Mediterranean region and two reconstructions at 5 and 15 Ma showing the position of volcanic edifices and plutons with an emphasis on the cases of the Cyclades and Elba Island addressed in this paper. These reconstructions are taken and modified from Romagny et al. (2020).

Figure 1

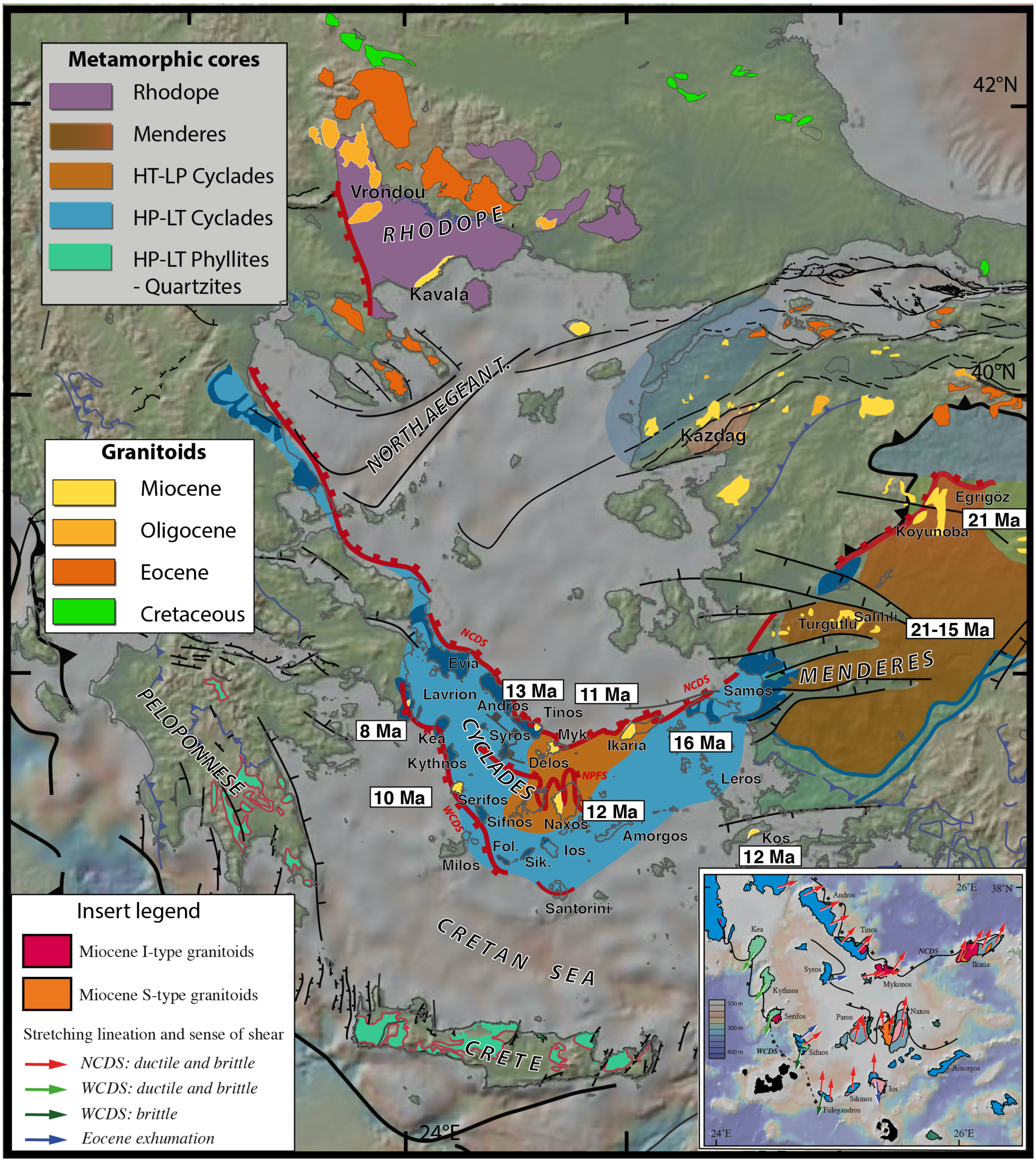

Figure 2: Tectonic map of the Aegean region showing the successive generations of granitoids since the late Cretaceous. Modified from Jolivet et al. (2015). Background topography was extracted from GeoMapApp.

Figure 2

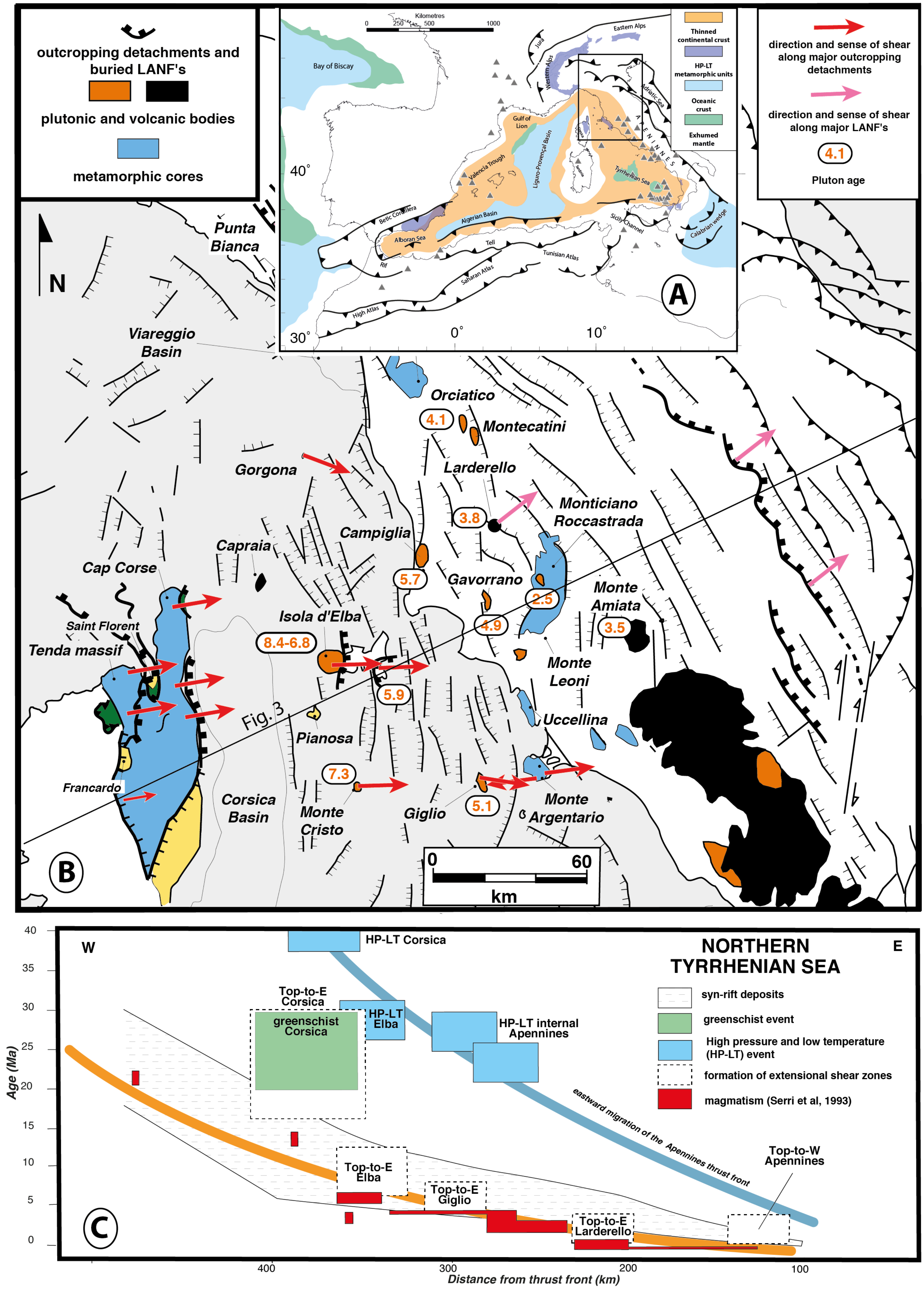

Figure 3: Tectonic map (A) of the Western and Central Mediterranean, (B) the northern Tyrrhenian region and Northern Apennines and (B) a diagram showing the evolution of the ages of syn-rift basins, metamorphic events and magmatism along a cross-section from Corsica to the Apennines, modified from Jolivet et al. (1998).

Figure 3

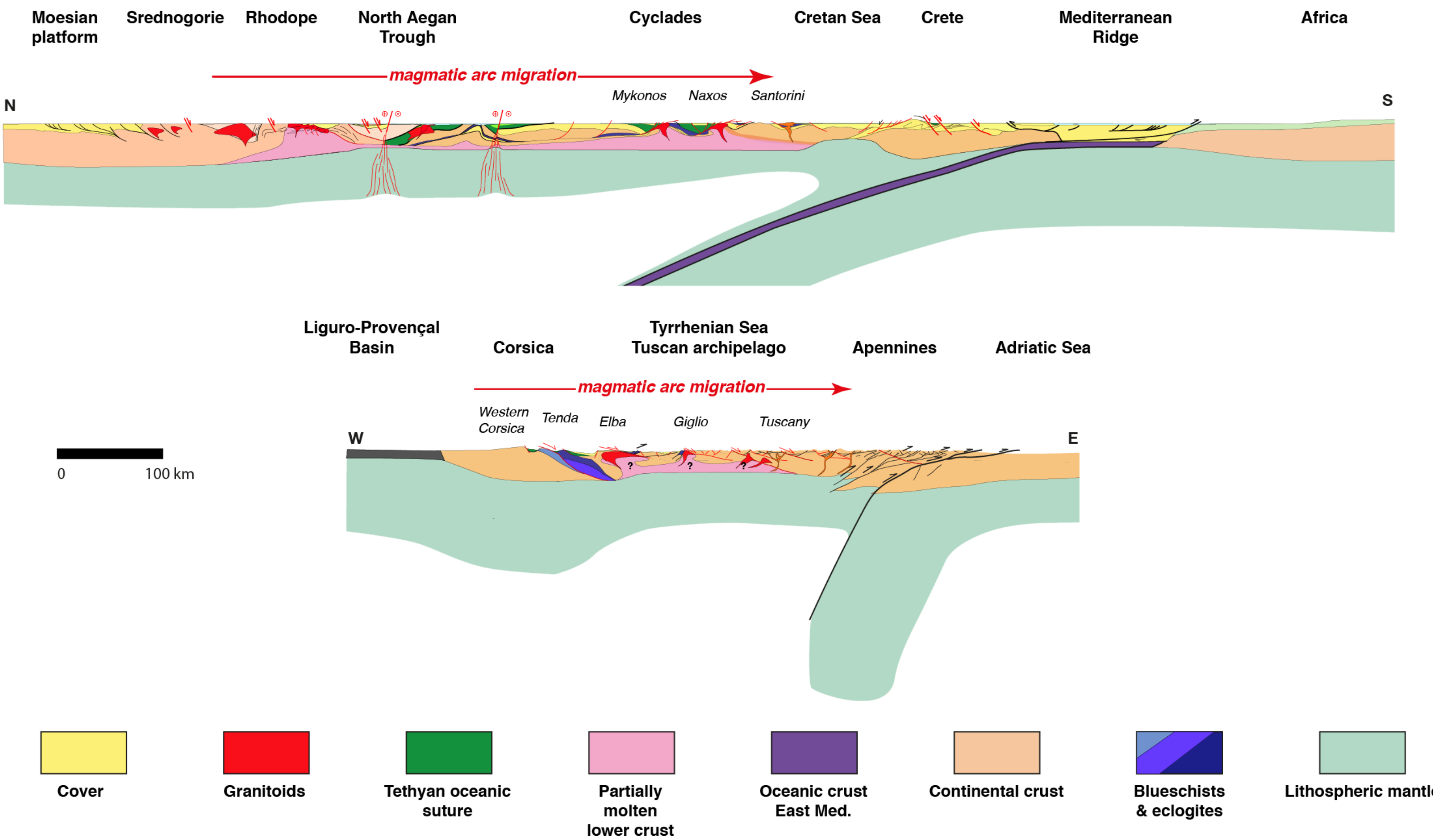

Figure 4: Two lithospheric-scale cross-sections of the Aegean domain (Jolivet and Brun, 2010) and the Northern Tyrrhenian Sea and the Apennines (Jolivet et al., 1998).

Figure 4

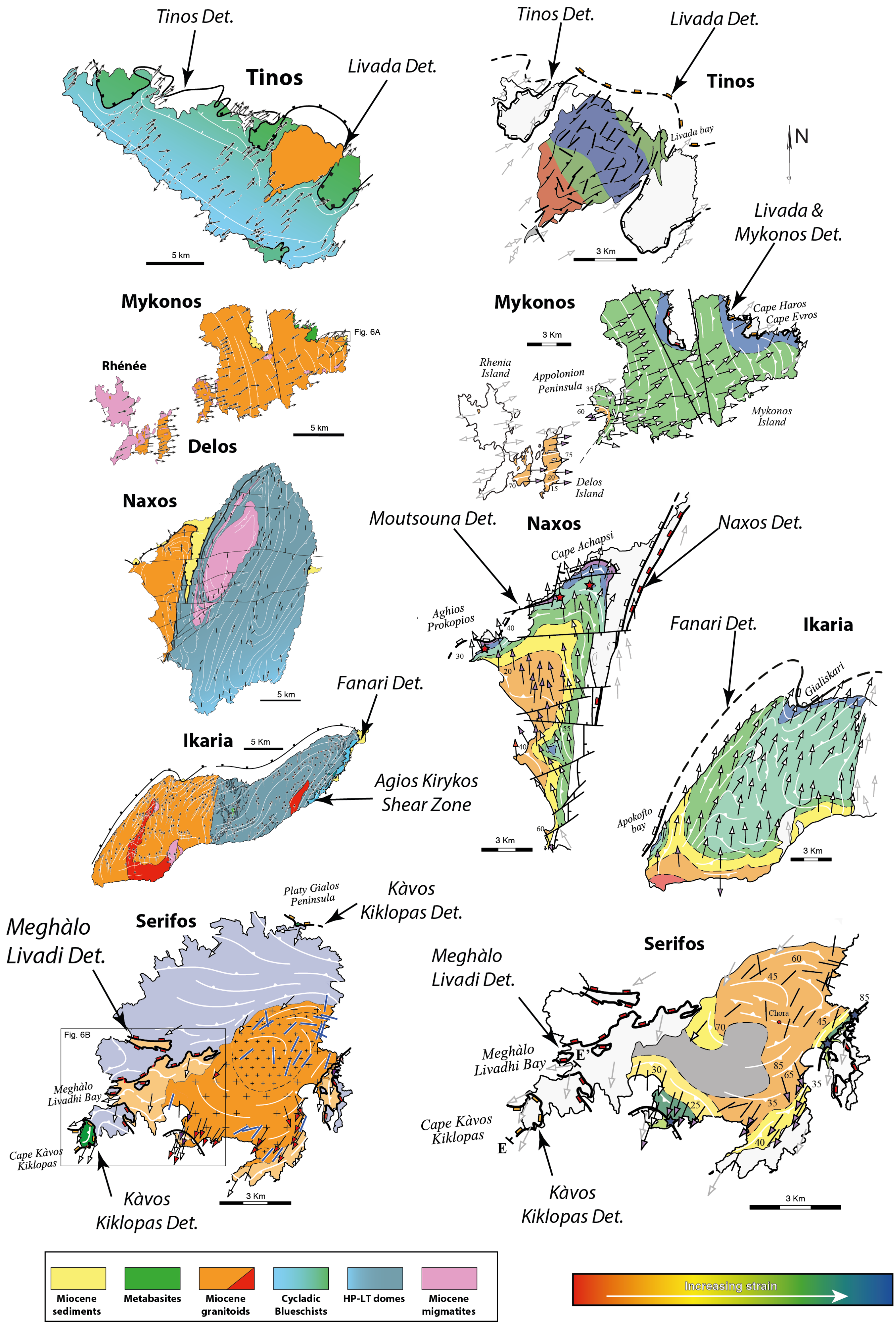

Figure 5: Five examples of the Aegean granitoids showing the interactions between deformation and intrusion, after Rabillard et al. (2017) and references therein. Maps of the left column show maps of the entire islands and the right column shows the internal fabrics of the plutons. These maps were obtained based on deformation grades observed in the field, a scale of grades was designed for each pluton to describe the gradients. Arrows show stretching lineations and sense of shear and black bars on the Tinos pluton shows the direction of the magnetic lineation.

Figure 5

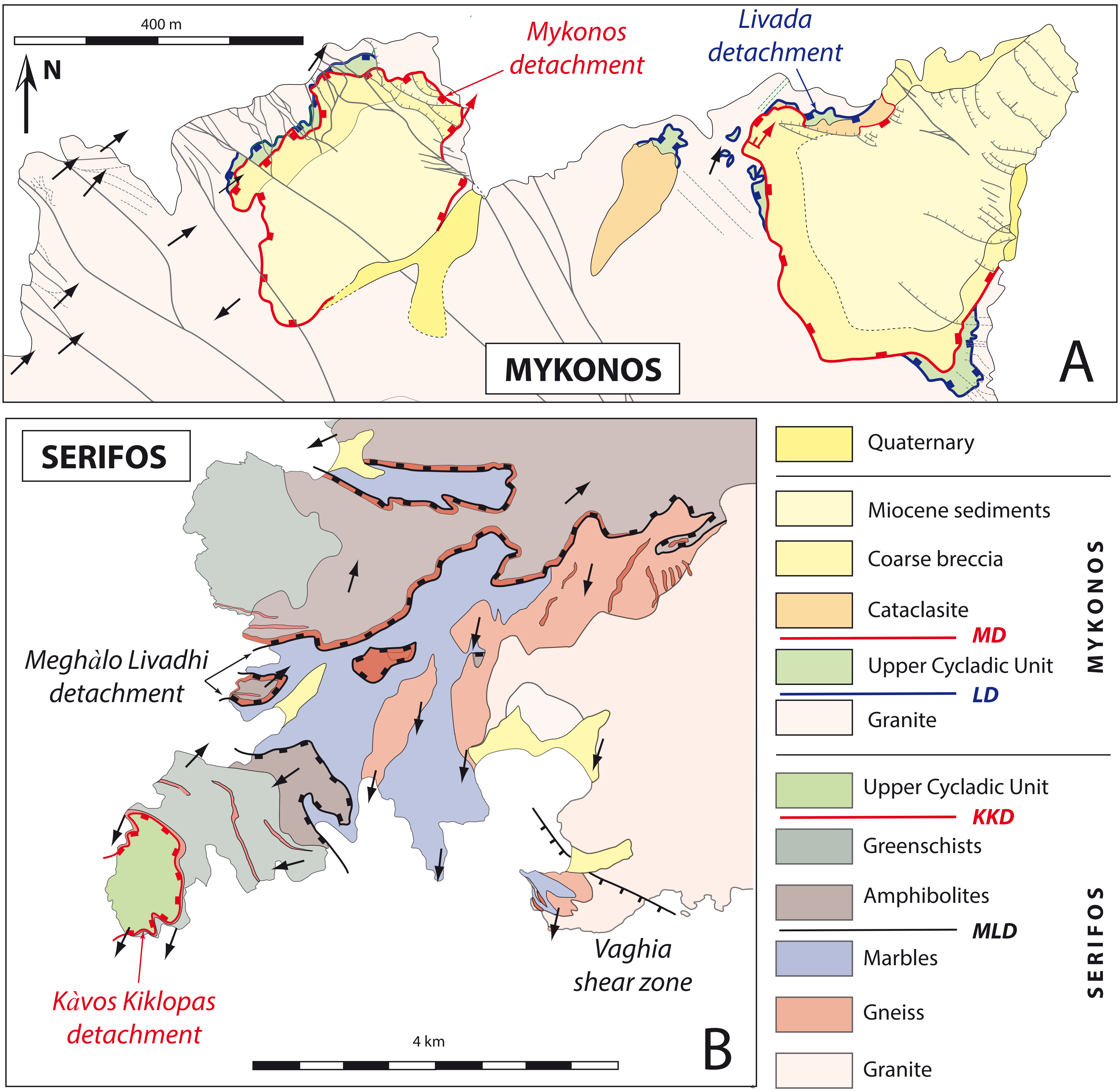

Figure 6: Details of the two detachments on Mykonos and Serifos. A: northeastern Mykonos (see location on figure 5), B: Southwest Serifos. The Mykonos (MD) and Livada (LD) detachments on Mykonos and the mineralized veins and normal faults (baryte and iron-hydroxides) – grey- are after Menant et al. (2013). The Kavos Kiklopas (KKD) and Meghalo Livadi (MLD) detachments on Serifos are after Grasemann and Petrakakis (2007) and Ducoux et al. (2016).

Figure 6

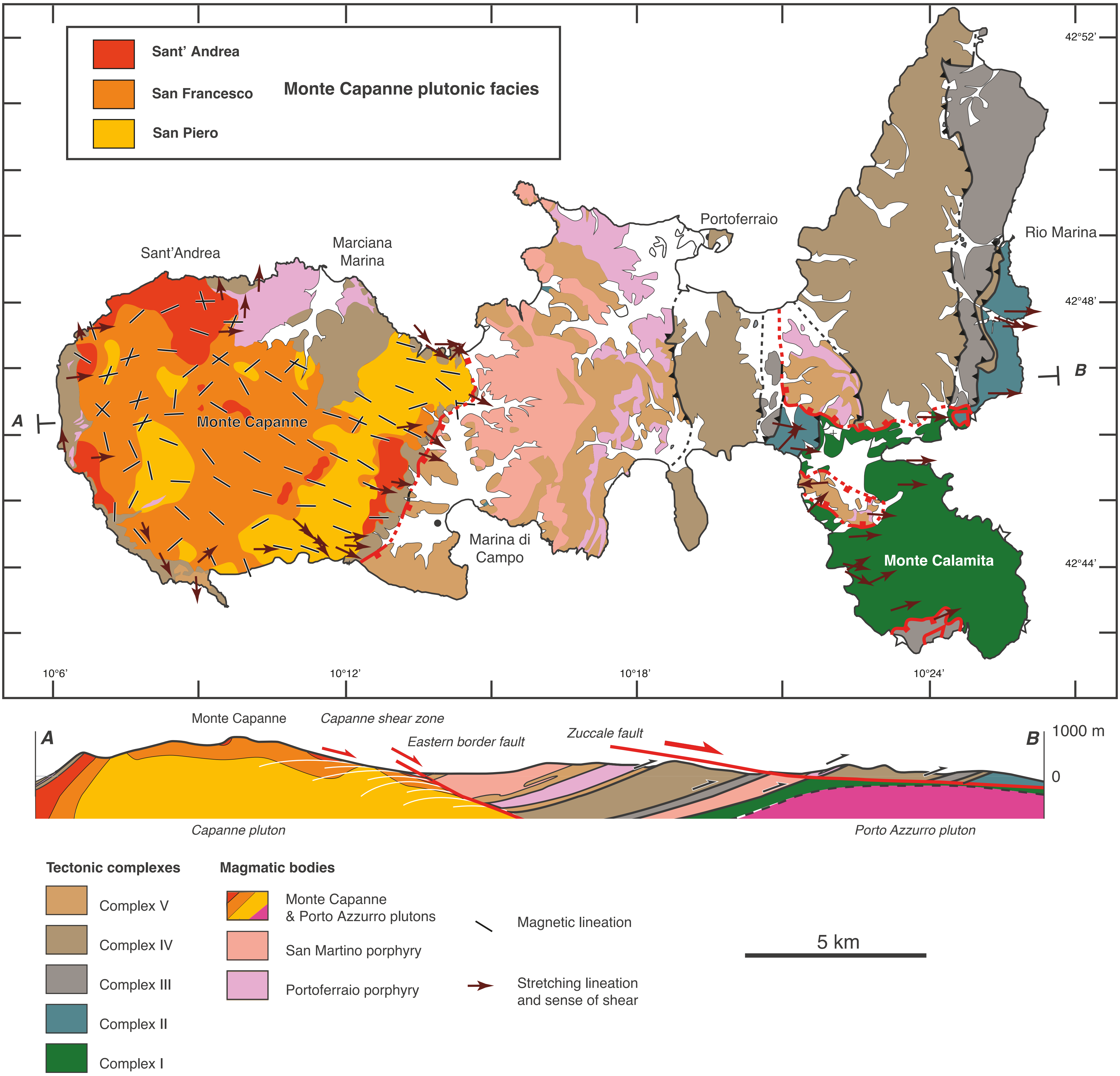

Figure 7: Tectonic map and cross-section of Elba Island showing the main tectonic units and the main extensional shear zones and detachments, modified after Bianco et al. (2015). Details of the internal structure of the Monte Capanne intrusions are reported based on Farina et al. (2010).

Figure 7

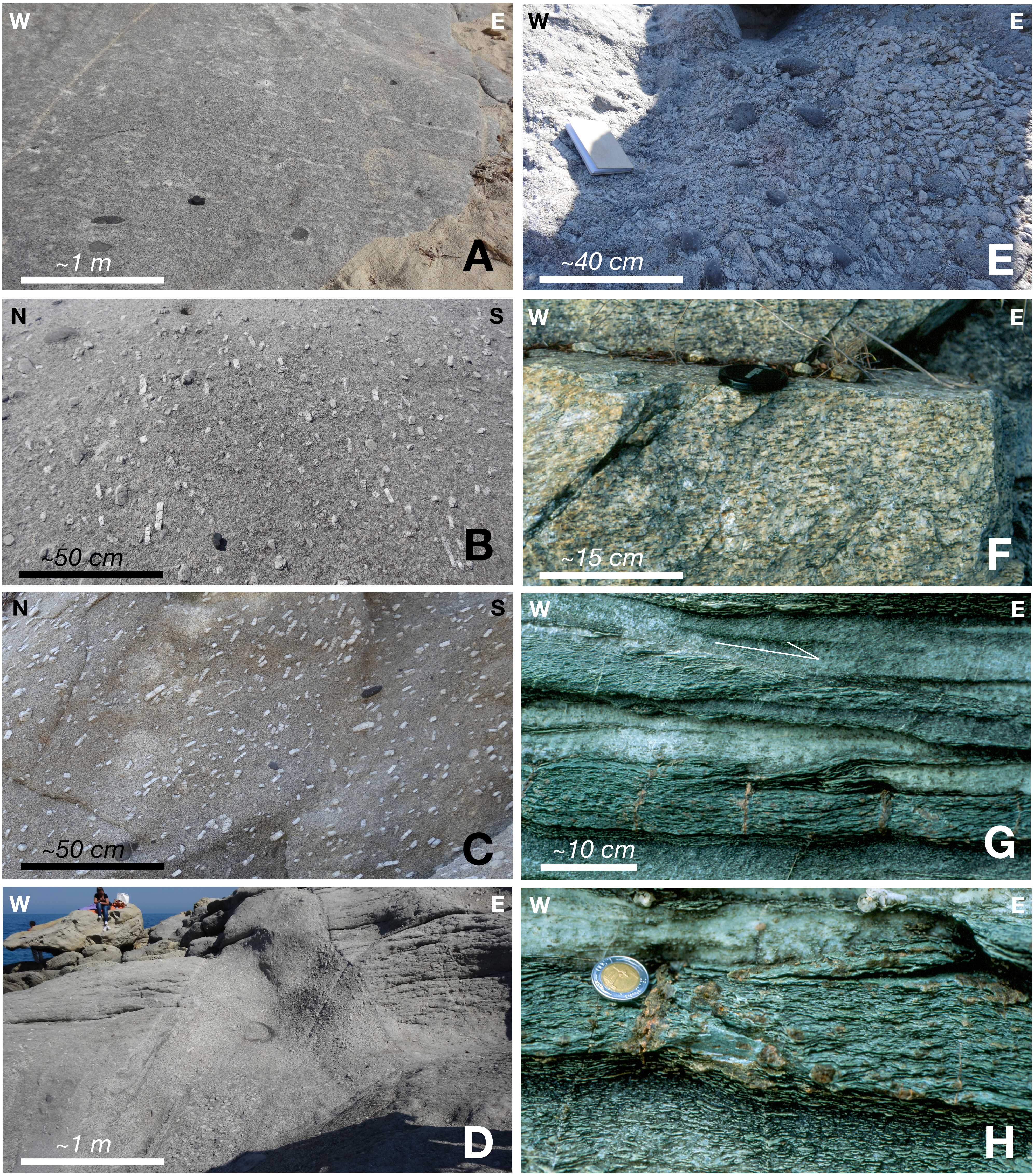

Figure 8: Photographs of the Sant' Andrea facies in the Monte Capanne pluton and of the deformation along the eastern margin of the pluton, in the pluton itself and in the contact metamorphic aureole. A: general view of the orientation of K-feldspar megacrysts and some mafic enclaves. B: Detailed view of the oriented K-feldspar megacrysts (horizontal plane). C: zoom on the orientation of K-feldspar megacrysts (vertical plane). D: Cotoncello dyke. E: cluster of K-feldspar megacrysts in the vicinity of the Cotoncello dyke. F: Mylonitic foliation within the Monte Capanne shear zone. G: Sigmoidal foliation and top-to-the-east sense of shear within the metamorphic aureole of the Monte Capanne pluton. H: detailed view of syn-kinematic contact

Figure 8

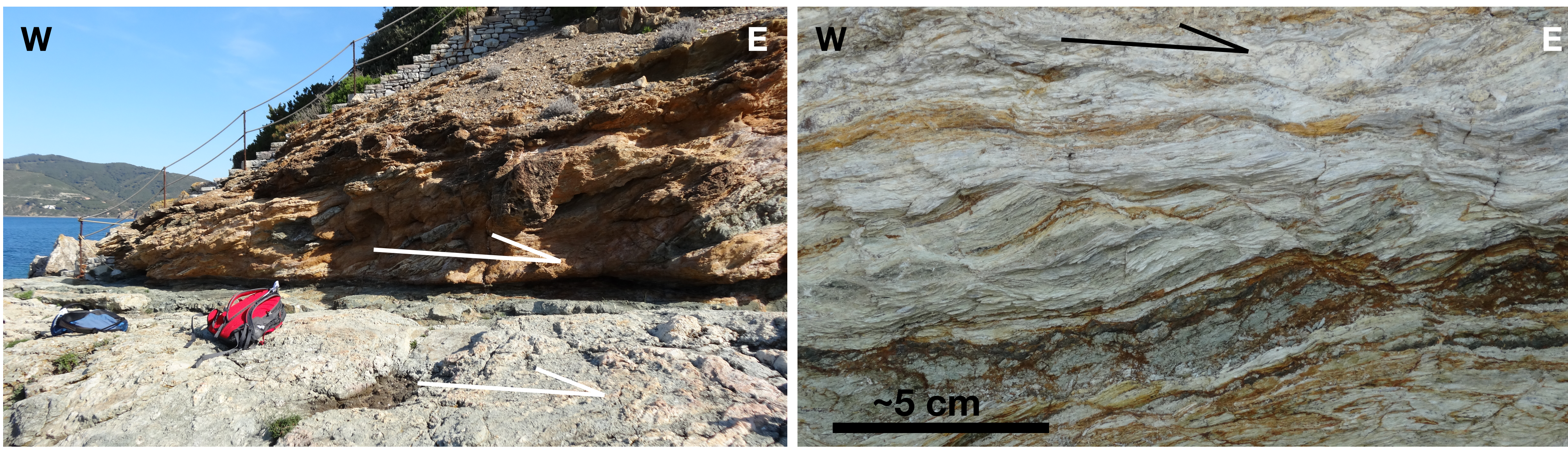

Figure 9: Photographs of the Zucalle detachment and its internal structure. Upper: overview of the detachment fault. Lower left: Detail of the contact zone and the truncated foliation in the hanging wall. Lower right: detail of the shear bands indicating top-to-the east kinematics.

Figure 9

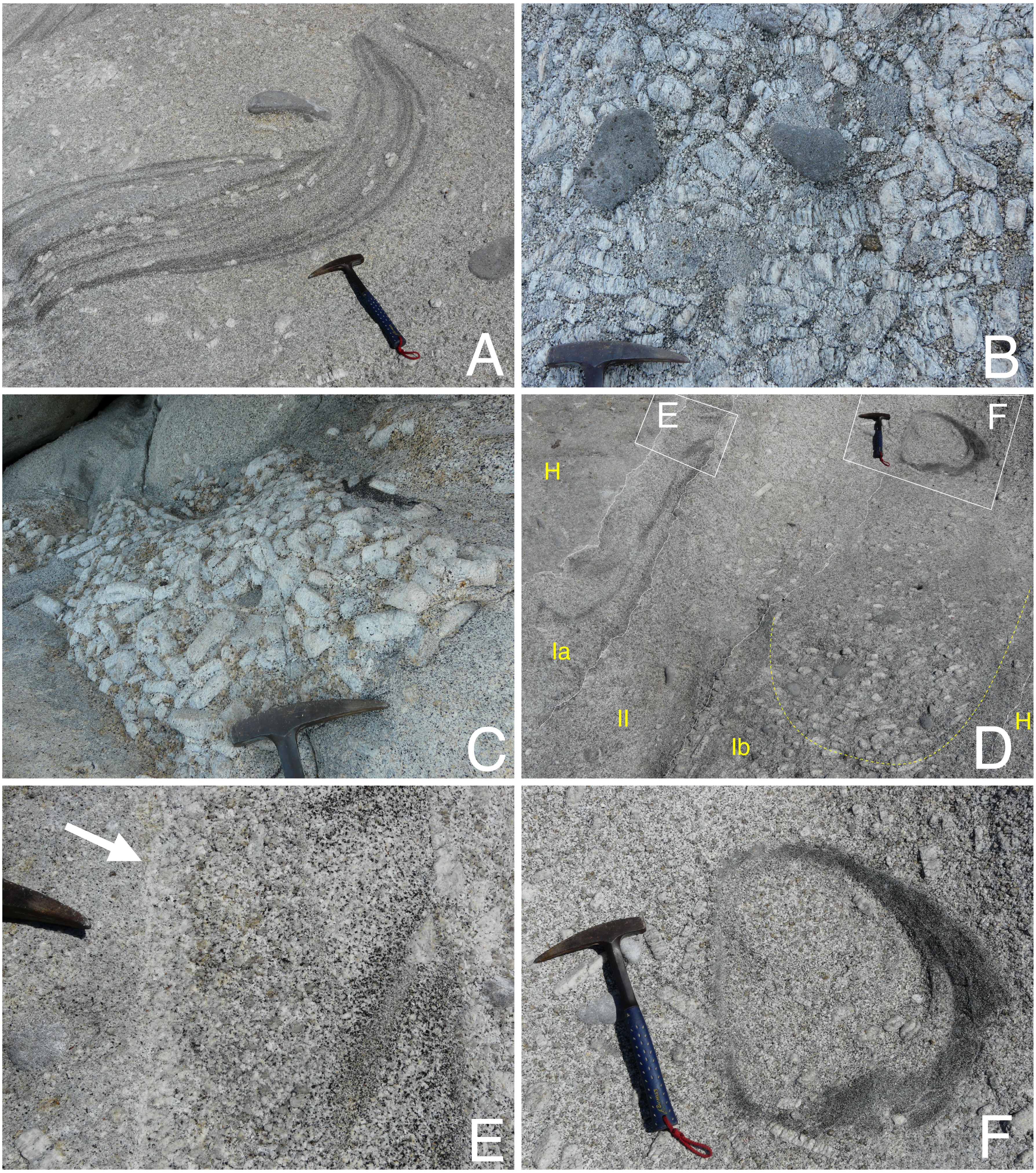

Figure 10: Photographs of the root zone of the Sant'Andrea facies in the melange zone in and around the Cotoncello dyke. A: Schlieren with cross-bedding. B: Mush zone with cluster of K-feldspar megacrysts and mafic enclaves. C: Isolated blob of mush zone with large K-feldspar megacrysts. D: Folded alternation of leucocratic and melanocratic layers with schlierens. E: Detail of D, schlieren. F: detail of D: schlieren tube.

Figure 10

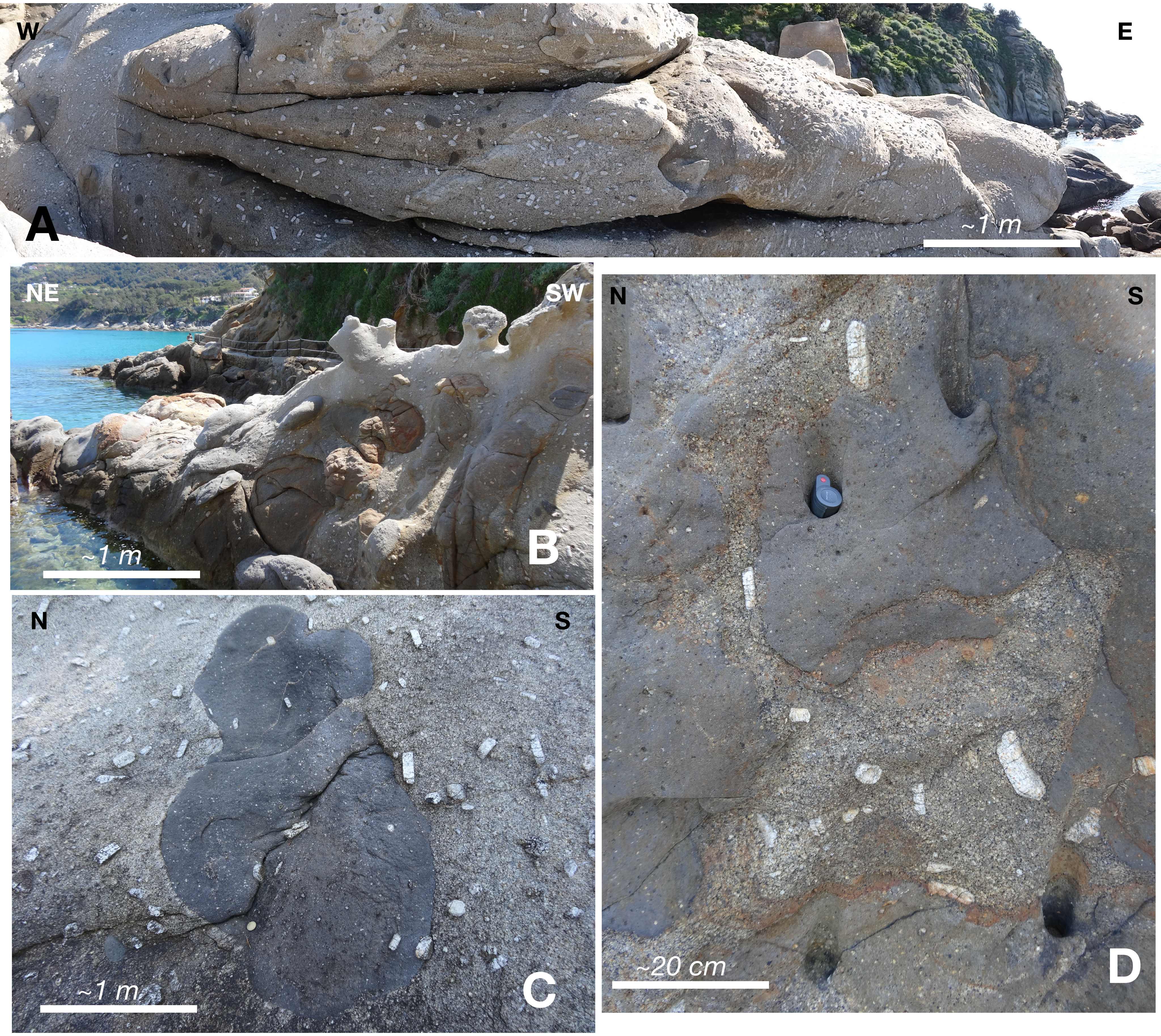

Figure 11: Photographs of large mafic enclaves and melange zones in the westernmost part of the Sant'Andrea facies showing the disorientation of K-feldspar megacrysts and melange facies (mingling).

Figure 11

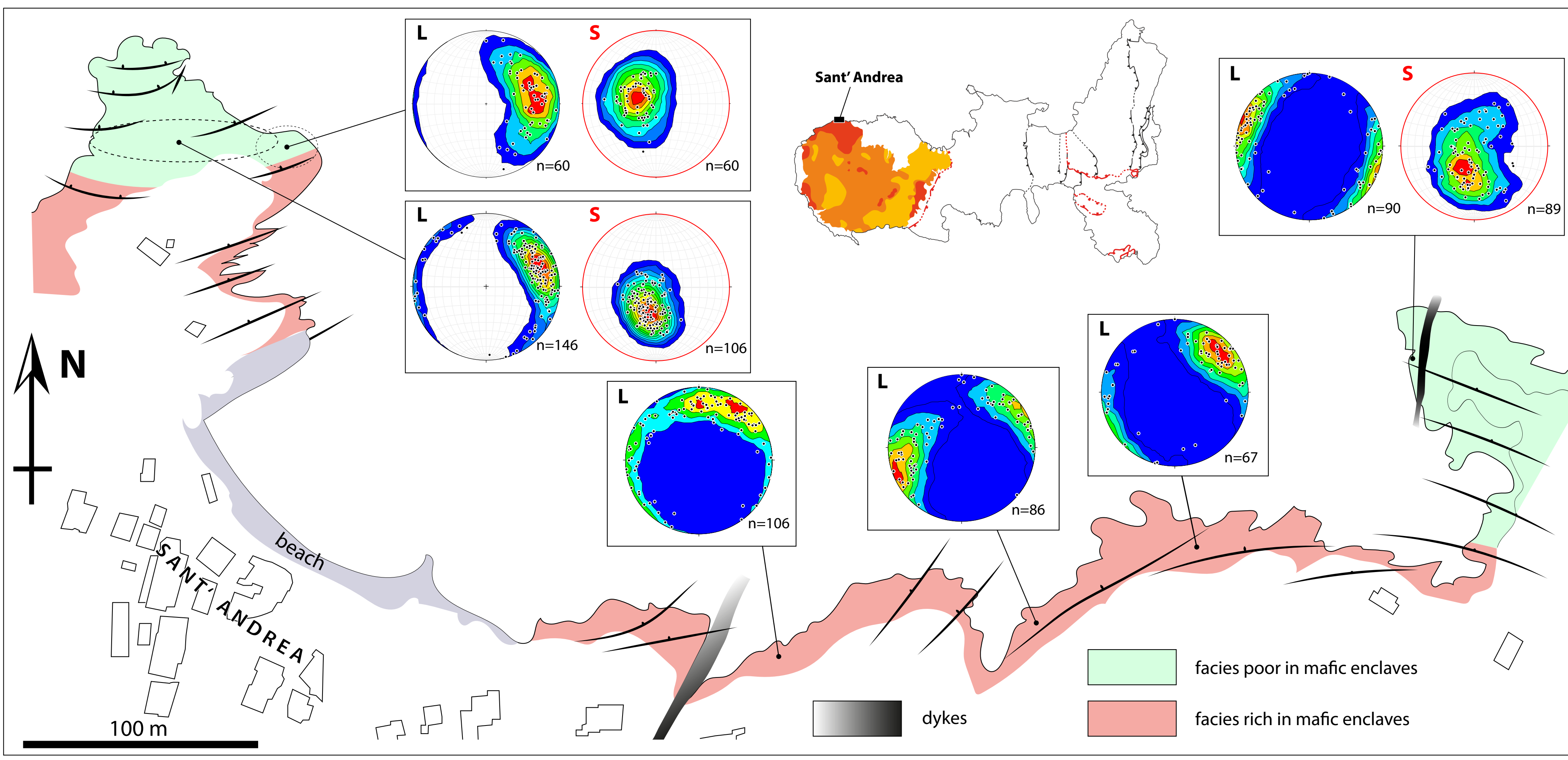

Figure 12: Detailed study of the orientation of K-feldspar megacrysts in the Sant-Andrea facies with foliation trajectories.

Figure 12

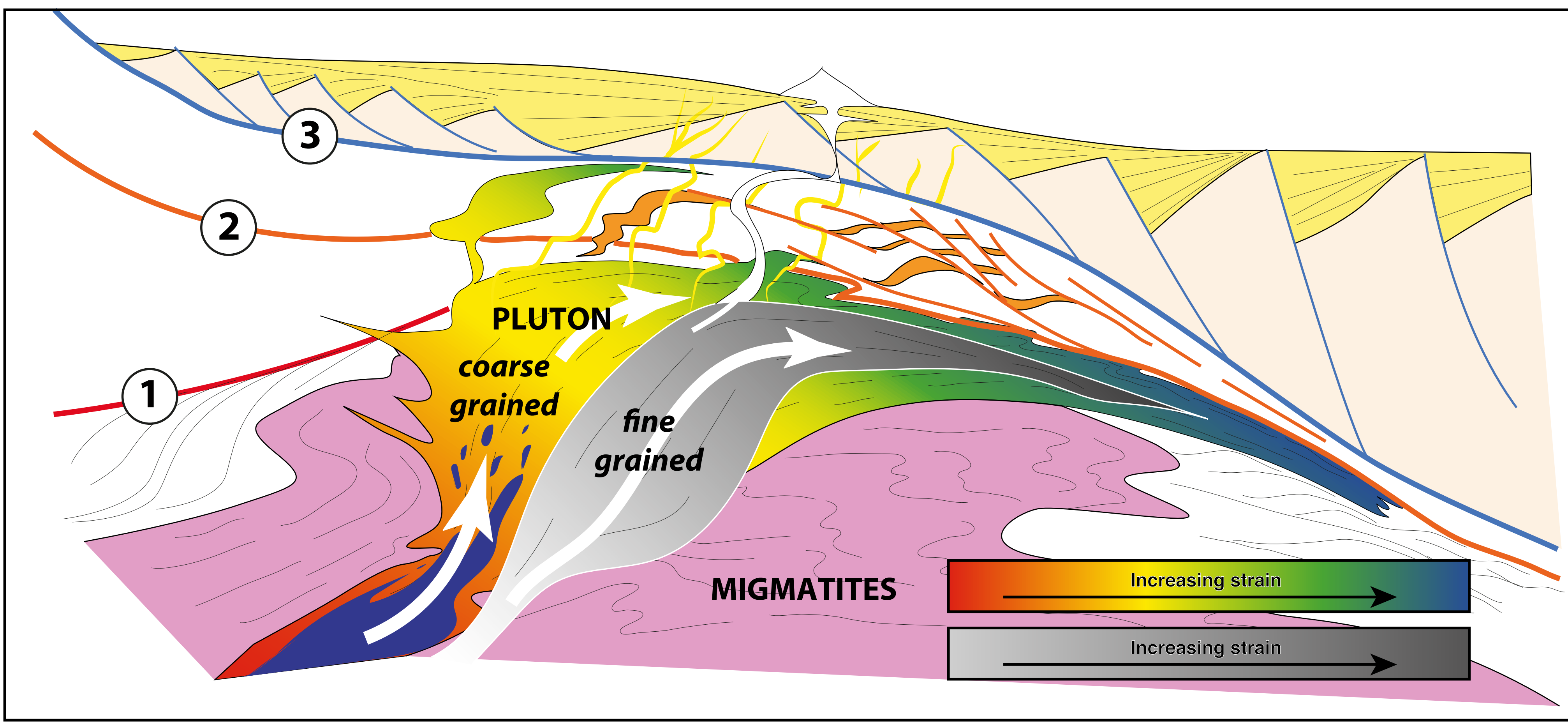

Figure 13: Schematic section showing a conceptual model of the relations between syn-kinematic plutons and the detachments, based on the examples of the Aegean and North Tyrrhenian plutons. Modified from Rabillard et al. (2017).

Figure 13

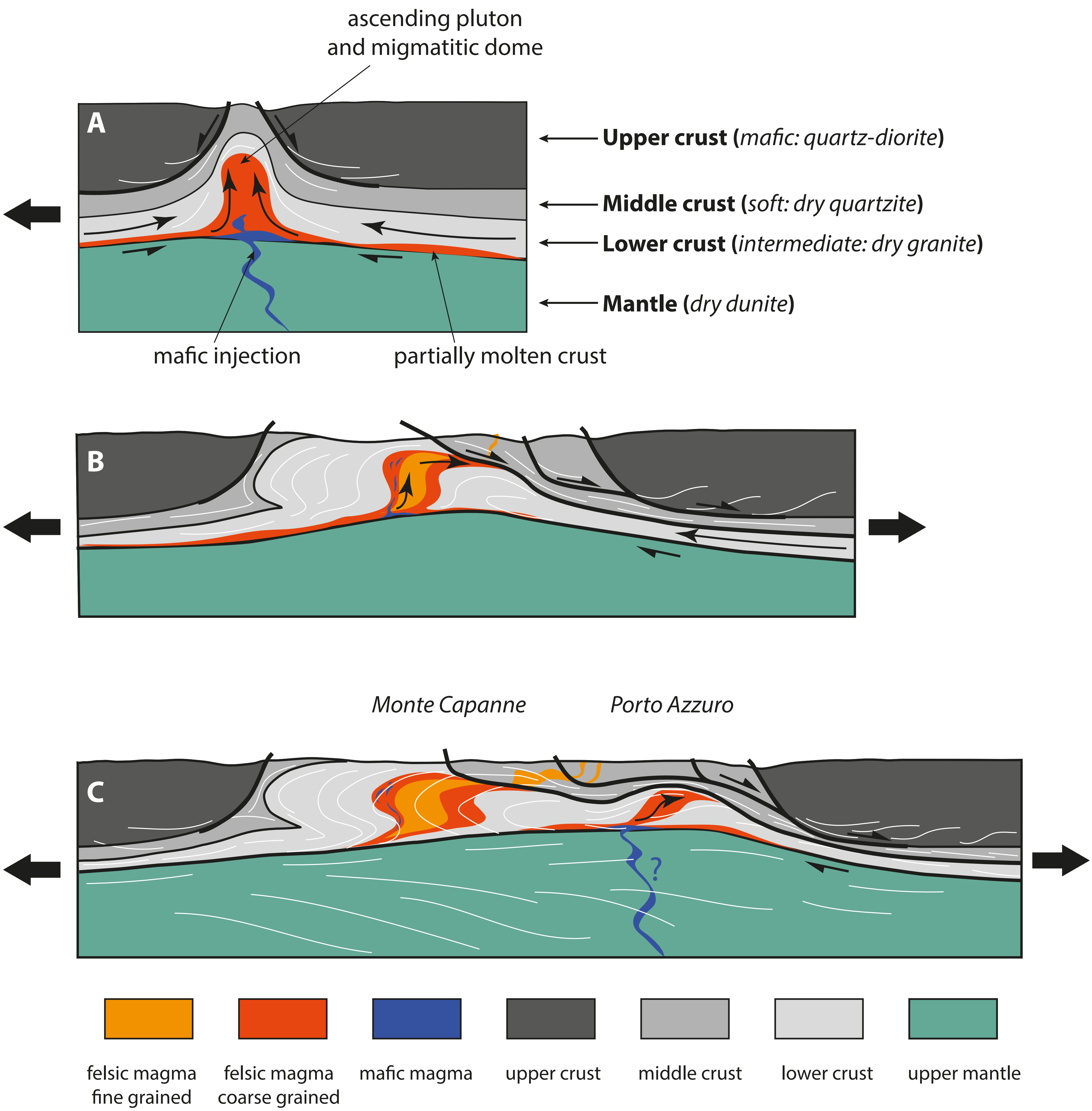

Figure 14: Conceptual model of the succession of events leading to the emplacement of a plutonic system below an active series of detachments, based on Huet et al. (2011) and Schubert et al. (2013).

Figure 14

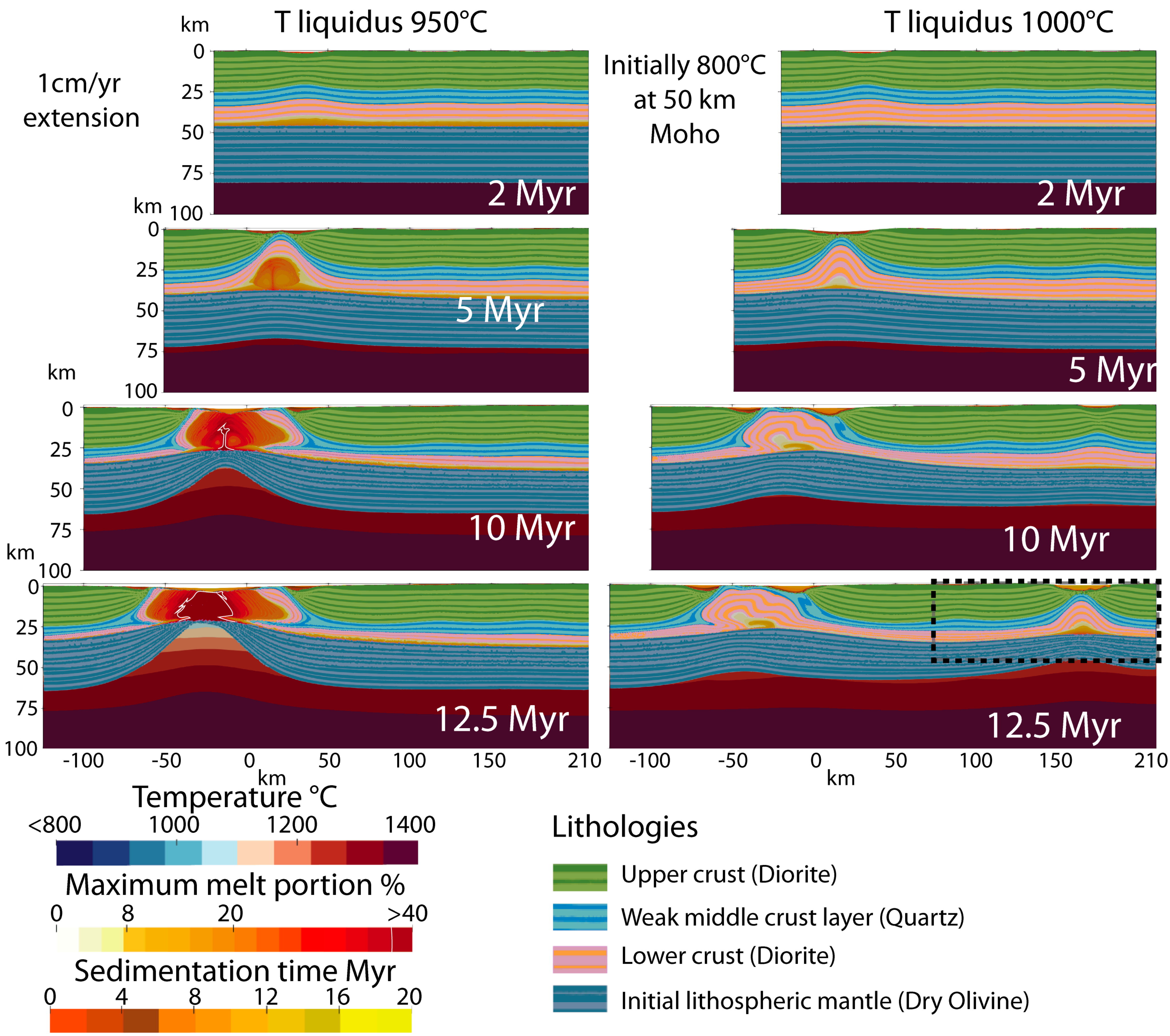

Figure 15: Snapshots of the numerical experiments with two different liquidus temperatures (950°C and 1000°C) from 2 to 12.5 Myr. White line limits the molten lower crust with melt ration above 40% (pluton).

Figure 15

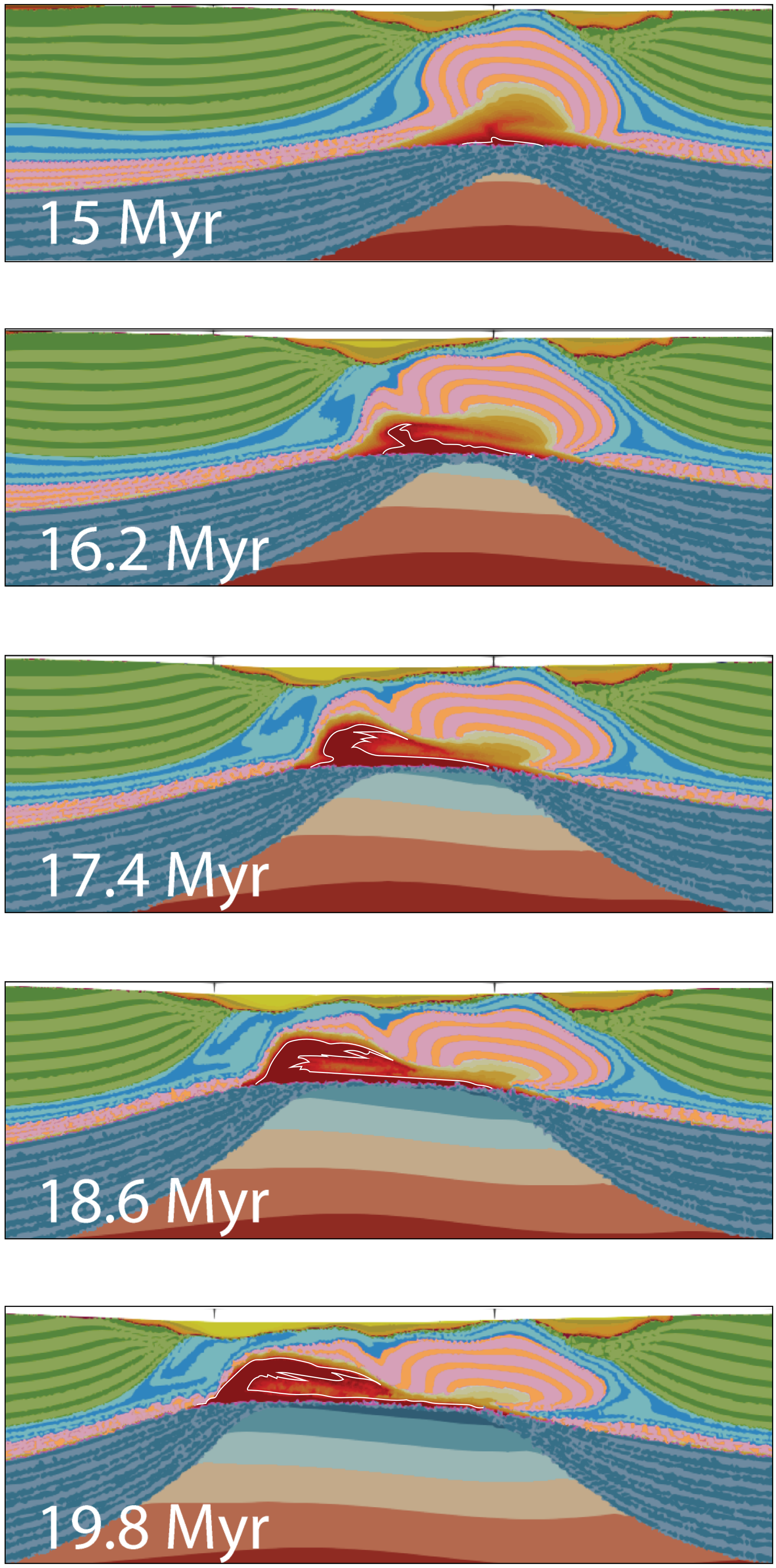

Figure 16: Zoom of the last 5 Ma of evolution of the model of figure 15 with a liquidus temperature of 1000°C from 15Myr to 19.8 Myr (black dotted rectangle on figure 15 for location).

Figure 16

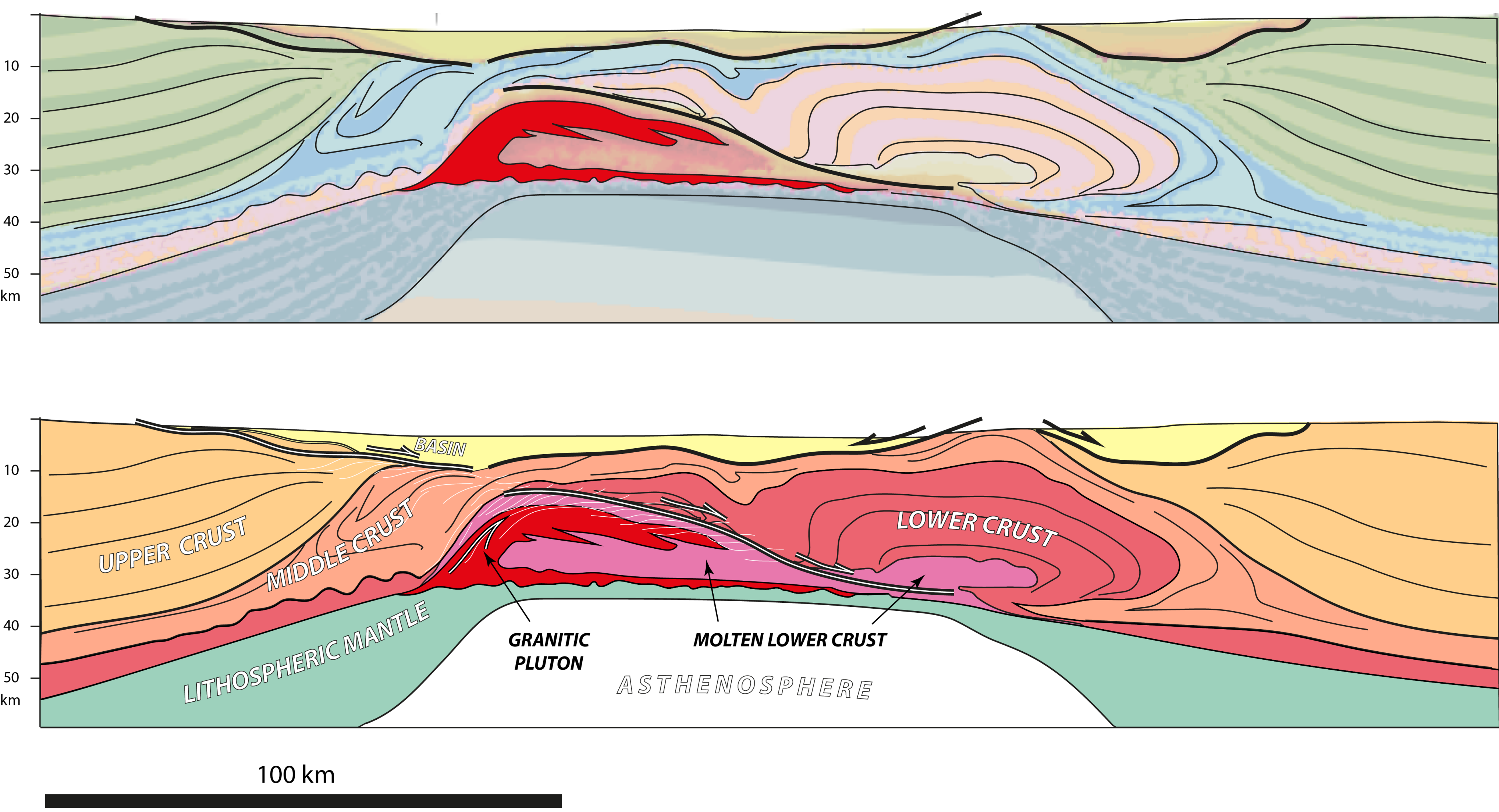

Figure 17: Structural cross-section based on the most evolved stage of the numerical model at 19.8 Myr.

Figure 17

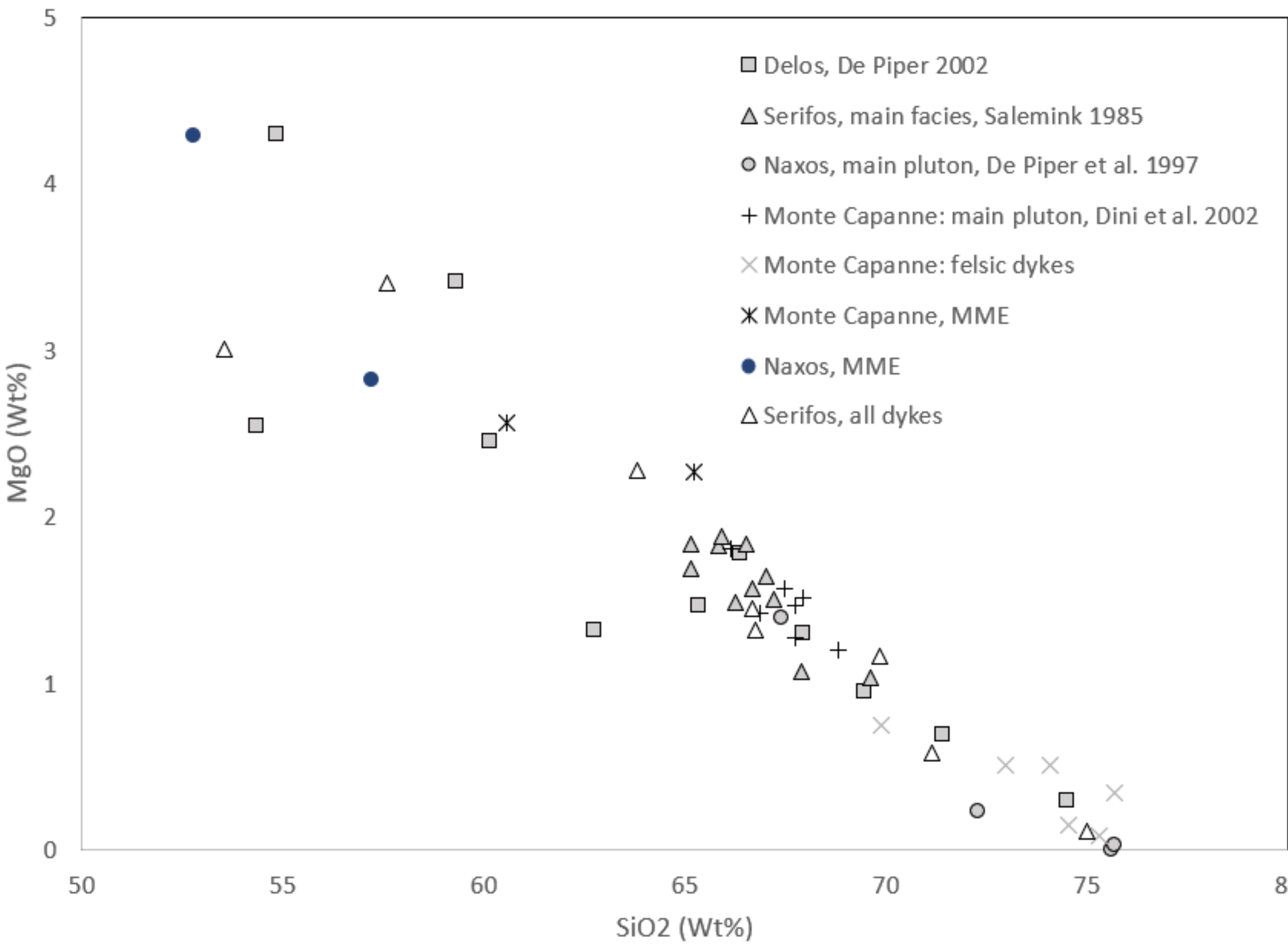
Delos, De Piper 2002
Serifos, main facies, Salemink 1985
Naxos, main pluton, De Piper et al. 1997
Monte Capanne: main pluton, Dini et al. 2002
Monte Capanne: felsic dykes
Monte Capanne, MME
Naxos, MME
Serifos, all dykes
MgO (Wt%)
SiO2 (Wt%)
0
1
2
3
4
5
50
55
60
65
70
75
80

Figure A1

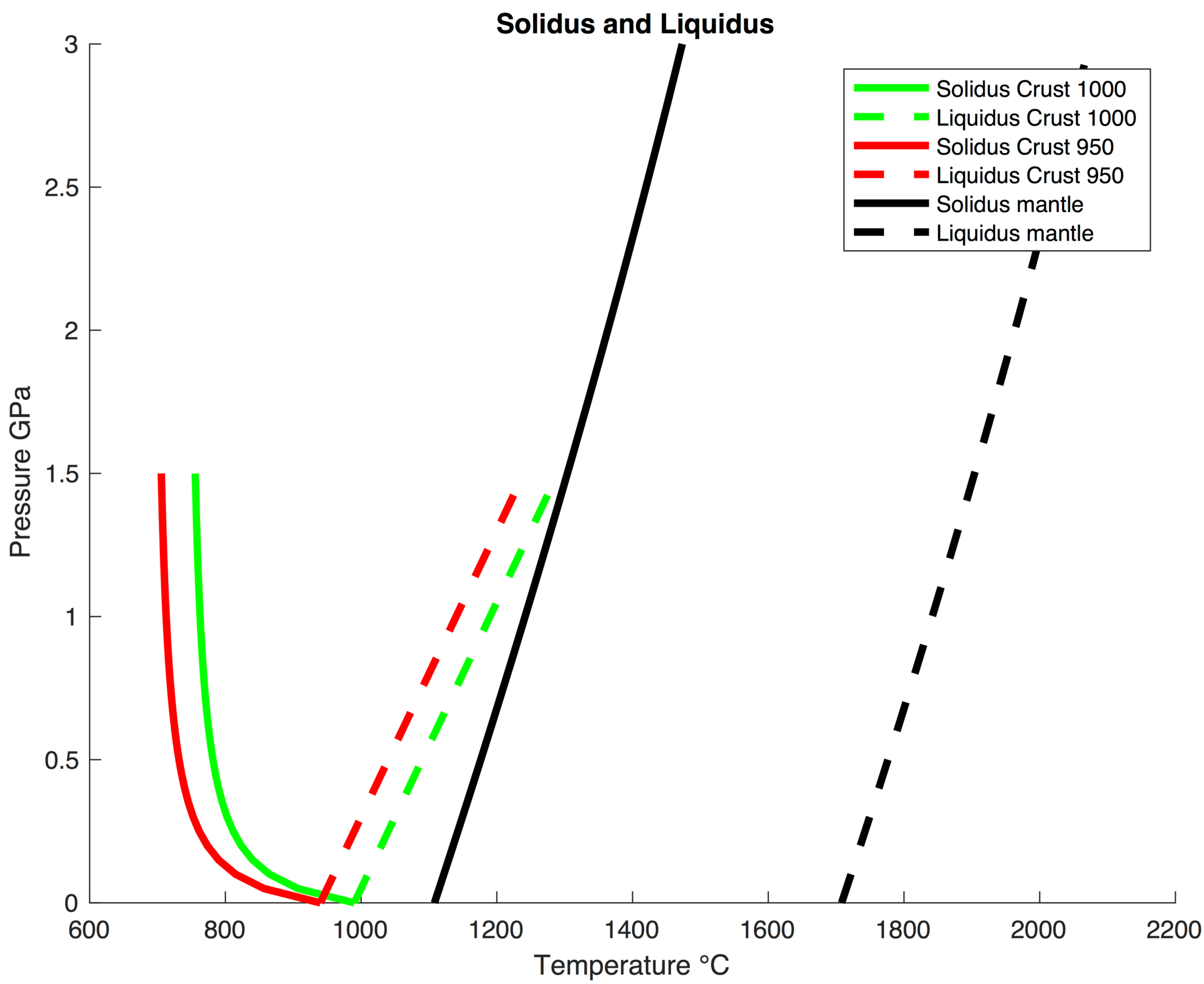
Solidus and Liquidus
Pressure GPa
Temperature °C
3
2.5
2
1.5
1
0.5
0
600
800
1000
1200
1400
1600
1800
2000
2200
Solidus Crust 1000
Liquidus Crust 1000
Solidus Crust 950
Liquidus Crust 950
Solidus mantle
Liquidus mantle

Figure A2